

Full-Potential Linearized Augmented Planewave Method

Stefan Blügel and Gustav Bihlmayer

Institute for Solid State Research, IFF
Research Centre Jülich, 52425 Jülich, Germany
E-mail: {s.bluegel, g.bihlmayer}@fz-juelich.de

The full-potential linearized augmented planewave (FLAPW) method has emerged as a widely used very robust and precise state-of-the-art *ab initio* electronic structure technique with reasonable computational efficiency to simulate the electronic properties of materials on the basis of density-functional theory (DFT). Due to the high precision it is widely accepted that it provides the density-functional answer to the problem. The shape of the charge density, the one-electron potential and the wavefunction is taken into account with high accuracy. The FLAPW method is an all-electron algorithm which is universally applicable to all atoms of the periodic table in particular to transition metals and rare-earths and to multi-atomic systems with compact as well as open structures. Due to the all-electron nature of the method, magnetism is included rigorously and nuclear quantities e.g. isomer shift, hyperfine field, electric field gradient (EFG), and core level shift are calculated routinely. Also open structures such as surfaces, clusters, organic and inorganic molecules as well as wires can be treated without problems. The capability of calculating atomic forces exerted on the atoms opens the path to structure optimization. In this chapter, a short introduction to first-principles methodology is given, the FLAPW-method is reviewed, modern extensions of the LAPW basis set are discussed, extensions of the method to geometries suitable to applications in nanoscience such as the film and wire geometries are presented. Details for the practical users e.g. important parameters controlling the accuracy of the results and an analysis of the CPU-time is given for the FLEUR-code, a particular implementation of the FLAPW method.

1 Introduction

Societal requests for environment prediction and protection, the durability of chemicals, the vision of new applications in information technology such as autonomous robots, bio-diagnostic systems, or faster information processing, as well as demands on the sustainable and efficient use of resources and energies translate in a huge demand on understanding, predicting, modeling and simulating the properties, chemical reactions, synthesis and growth processes of emergent quantum materials. Modern solid state materials have a multiplicity of novel properties exhibiting for example a rapid phase response to external stimuli such as light, pressure, magnetic field or electrical conductivity so that manifold uses are possible even today or can be expected for the future. Materials of this sort are often multicomponent systems such as magnetic tunneljunctions (e.g. NiMnSb|MgO|Co₂MnSn), high-temperature superconductors (e.g. HgBa₂Ca₂Cu₂O₈), or perovskite-type materials with complex magnetic structures. A particularly rich arsenal of assets for material design and tailoring of material properties is provided when the surface of materials is provided as templates for fabrication. Nanostructures down to the atomic scale made of single atoms or of small molecules can be manufactured to form chains and clusters or structures with specific electronic properties by employing the tip of scanning tunneling microscope (STM) or relying on the instruments of self-assembly. Nanostructured thin film systems are decisive functional units in electronic devices, sensors and in biological systems. The existence of particular surface and interface alloys and the complex interplay between morphological,

structural, magnetic and electronic features in nanostructured systems stand as examples for a wide field of phenomena which are largely not understood, while offering exceptional technological opportunities at the same time.

During the past ten years, first-principles calculations based on the density-functional theory (DFT)¹ in the local (spin-) density approximation (LDA) or in the generalized gradient approximation (GGA) (for a review see Ref.²⁻⁴) emerged as the most powerful framework to respond to the demands mentioned above on a microscopic level. By first-principles or *ab initio*, respectively, is meant, that the parameters of the theory are fixed by the basic assumptions and equations of quantum mechanics and, for our discussion, density-functional theory. The overwhelming success of the density-functional theory for the description of the ground-state properties of large material classes including insulators, semiconductors, semimetals, half-metals, simple metals, transition-metals and rare-earths in bulk, at surfaces and as nanostructures makes it the unchallenged foundation of any modern electronic structure theory. The wide applicability combined with the predictive power of the approach turned it to the “standard model” in material science. In principle, the only input needed for the theory are the atomic numbers of the constituent atoms of a system, all other properties follow as a direct consequence of the density-functional equations. In practice, the definition has to be modified since one is always limited to some set of model systems. These limitations might include system size, crystal structure, neglect of disorder, low or zero temperature, or any number of other restrictions on the “phase space” to probe. While some of these restrictions and limitations are burdensome, the goal of calculations is not merely to obtain numbers, but rather insight. By focusing on well-defined, but restricted models, by working on chemical trends rather than on isolated case studies, by investigating systems in hypothetical non-equilibrium structures or follow simulations in idealized environments, which may not be realized in experiments, one is able to develop different levels of understanding of the system in question and may hopefully learn which aspects of the problem are important. In the density-functional theory we work in an effective one-particle picture: the wavefunctions are solutions of the Kohn-Sham equations and the interaction of the particles is taken into account by a self-consistent field, which depends on the density of the particles. The adequacy and limitations of this approach have been extensively discussed in the literature and pioneered by^{5,6}. Successful extensions of the theoretical framework treat quasiparticle excitations of weakly correlated electron systems by many-body perturbation theory based on Green-function techniques in the so-called *GW* approximation for the electronic self-energy (for details see chapter “Many-Body Perturbation Theory: The *GW* Approximation” by C. Friedrich and A. Schindlmayr) or by time-dependent density-functional theory (TDDFT)^{7,8}. The treatment of strongly correlated electron systems is currently being explored investigating the LDA+U approximation, the optimized potential method (OEP)⁹ and by combining the dynamical mean field theory (DMFT)^{10,11} with the LDA.

In this chapter, we review the full-potential linearized augmented planewave (FLAPW) method^{12,13}, to solve the density-functional equations for a crystalline solid, ultrathin film and one-dimensional system (a review is given by D. J. Singh¹⁴). The method originates from the APW method proposed by Slater¹⁵⁻¹⁷. Great progress of the APW methodology was achieved as the concept of linear methods¹⁸⁻²², was introduced by Andersen and first applied by Koelling and Arbman using a model potential within the muffin-tin approximation. The linearized APW (LAPW) method reconciled the linear-algebra formulation

of the variational problem with the convergence properties of the original formulation and allowed a straight forward extension of the method to the treatment of crystal potentials of general shape. The treatment of the potential and charge density without shape approximation^{23,24} and the implementation of the total energy¹³ led to the development of FLAPW bulk^{12,24–30} film codes^{12,30–32}. It was during this time that the power and accuracy of the method were demonstrated to the community, largely through a series of calculations of surface and adsorbate electronic structures (for a review see Wimmer *et al.*³³). These and other demonstrations established the FLAPW method as the method of choice for accurate electronic structure calculations for a broad spectrum of applications.

Constant conceptual and technical developments and refinements such as the proposal and implementation of the scalar-relativistic approximation (SRA)³⁴, the spin-orbit interaction by second variation³⁶, and the possibility to calculate forces^{37,38} acting on the ions to carry out structure optimizations, quasi-Newton methods³⁹ to accelerate the self-consistency iterations, the iterative diagonalization techniques^{40–42}, the proposal of a new efficient basis sets, the LAPW+LO⁴³ and APW+lo⁴⁴ basis, in which the APW basis is amended by local orbitals (lo), the extension of the method to non-collinear magnetism⁴⁵, to the wire geometry⁴⁶, to calculations of the quasiparticle self-energy in the *GW* approximation⁴⁷, and the recent formulation and application of the scattering problem in semi-infinite crystals^{48–50} has made APW-like methods, and for our discussion the FLAPW method, a robust, versatile and flexible method, at reasonable computational expense. It is an all-electron method, that means, one works with a true crystal potential, which diverges as $1/r$ at the nucleus, as opposed to the pseudo-potential (for a review see Ref.^{51,52}), in which the singularity is removed. Due to the all-electron nature of the method, magnetism is included rigorously and nuclear quantities⁵³ e.g. isomer shift, hyperfine field, electric field gradient (EFG), and core level shift are calculated routinely. The method and the breadth of applications has benefited from the large growth of available computing power and parallelization strategies.

This chapter starts with a quick overview to the Kohn-Sham ansatz outlining the general aspects of the first-principles methodology followed by an introduction of the APW-like concepts to solve the Kohn-Sham equation for a periodic solid. Then, the FLAPW method is described in detail for bulk solids followed by a short description of adaptations of the FLAPW methods to systems of reduced dimensions, the film and wire geometry. Finally an analysis of the CPU-time distribution across the different steps of an *ab initio* calculation with an FLAPW program is presented. Strategies to speed-up the calculations in the light of symmetry and parallelization concepts are described.

2 Solving the Kohn-Sham Equations in a Nutshell

2.1 Total Energy and Force

In the density-functional theory, the total energy $E[\{\mathbf{R}\}, \{\psi_i\}]$ of a system of interacting atoms and electrons is a functional of the atomic positions $\{\mathbf{R}\}$ and the electron density $n(\mathbf{r})$. The electron density can be expressed in terms of M occupied single-particle orbitals $\psi_i(\mathbf{r})$:

$$n(\mathbf{r}) = \sum_{i(occ)}^M |\psi_i(\mathbf{r})|^2, \quad (1)$$

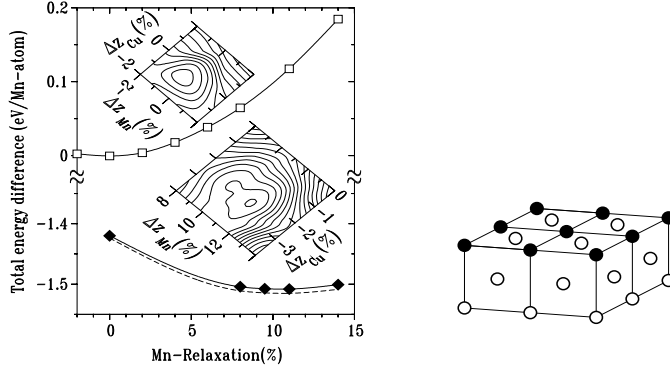


Figure 1. Example: structural optimization of Mn and Cu surface atoms in a Cu(100)c(2 × 2)Mn surface alloy. Right figure: Schematic representation of the substitutional surface alloy film of one monolayer thickness (● indicates the Mn atoms) grown as overlayer on a fcc (001) substrate (○). Left figure: Total energy per Mn atom vs. the buckling relaxation Δz_{Mn} of Mn in relative units with respect to the theoretical interlayer spacing of Cu, $d_{Cu} = 1.76$ Å. The open squares represent the nonmagnetic and the solid diamonds the ferromagnetic results. The solid lines (for Cu atoms fixed at the ideally terminated positions $\Delta z_{Cu} = 0$) and dashed line (the top Cu atom is always at its optimally relaxed position) are the fitting polynomials. The upper (lower) inset shows the contour plot of the nonmagnetic (ferromagnetic) total energy with respect to the buckling of Mn and Cu. The minimum, which determines the optimal structure is found in the inner circle. The contour interval is 1 meV. The energy of the nonmagnetic solution at 0% relaxation was chosen as the origin of the total energy scale (taken from Ref.⁵⁴).

where i labels the states. If the total energy functional $E[\{\mathbf{R}\}, \{\psi_i\}]$ is minimized with respect to the electronic degrees of freedom $\{\psi_i\}$, we recover the Born-Oppenheimer surface $\Phi[\{\mathbf{R}\}]$:

$$\Phi[\{\mathbf{R}\}] = \min_{\{\psi_i\}} E[\{\mathbf{R}\}, \{\psi_i\}], \quad (2)$$

on which the atoms move. The derivative of $\Phi[\{\mathbf{R}\}]$ with respect to the atomic position \mathbf{R}^μ gives the force \mathbf{F}^μ ,

$$\mathbf{F}^\mu = -\nabla_{\mathbf{R}^\mu} \Phi[\{\mathbf{R}\}] \quad (3)$$

exerted on the atom μ , which ties electronic structure to structural optimization and molecular dynamics calculations. The energy functional is divided into several terms:

$$E[\{\mathbf{R}\}, \{\psi_i\}] = E_{kin}[\{\psi_i\}] + E_H[\{\psi_i\}] + E_{xc}[\{\psi_i\}] + E_{ext}[\{\mathbf{R}\}, \{\psi_i\}] + E_{ion}[\{\mathbf{R}\}], \quad (4)$$

where E_{kin} is the kinetic energy of non-interacting electrons, E_H is the Hartree energy, i.e. the classical Coulomb energy of the electrons, and E_{xc} is the exchange-correlation energy which contains terms coming from the Pauli principle (exchange hole), from correlations due to the repulsive Coulombic electron-electron interaction and from the contribution to the kinetic energy of interacting electrons³. E.g. In the local density approximation $E_{xc}[n]$ is written in the form $E_{xc}[n] = \int d\mathbf{r} n(\mathbf{r}) \varepsilon_{xc}(n(\mathbf{r}))$. Then, E_{ext} is the interaction energy of the electrons with the ions, e.g. described by the $1/r$ potential as in all-electron methods or by pseudo-potentials, and E_{ion} is the classical Coulomb energy of the ions.

2.2 The Kohn-Sham Equations

The single-particle wavefunctions $\psi_i(\mathbf{r})$ are obtained by minimization of the total energy with respect to the wavefunctions subject to the normalization constraint

$$\int d\mathbf{r} |\psi_i(\mathbf{r})|^2 = 1. \quad (5)$$

This leads to the Kohn-Sham equations⁵⁵, an eigenvalue problem for the eigenfunctions $\psi_i(\mathbf{r})$ and the eigenvalues ε_i :

$$\hat{H}[n] \psi_i[n] = \varepsilon_i[n] \psi_i[n], \quad (6)$$

where all quantities depend on the electron density n . According to the form of the total energy Eq.(4), the Hamiltonian \hat{H} is a sum of corresponding terms and the eigenvalue problem is written in the form:

$$(\hat{T}_0 + \hat{V}_{\text{ext}} + \hat{V}_H + \hat{V}_{\text{xc}}) \psi_i(\mathbf{r}) = \varepsilon_i \psi_i(\mathbf{r}) \quad (7)$$

In the real space representation the individual terms are the following:

$$\text{kinetic energy :} \quad \hat{T}_0 = -\frac{\hbar^2}{2m} \Delta_{\mathbf{r}} \quad (8)$$

$$\text{external-potential :} \quad V_{\text{ext}}(\{\mathbf{R}\}, \mathbf{r}) = \sum_{\mu} \frac{e^2 Z^{\mu}}{|\mathbf{r} - \mathbf{R}^{\mu}|} \quad (9)$$

$$\text{Hartree potential :} \quad \Delta_{\mathbf{r}} V_H(\mathbf{r}) = 4\pi e^2 n(\mathbf{r}) \quad (10)$$

$$\text{xc-potential (LDA) :} \quad V_{\text{xc}}(\mathbf{r}) = \frac{\delta}{\delta n(\mathbf{r})} \int d\mathbf{r} n(\mathbf{r}) \varepsilon_{\text{xc}}(n(\mathbf{r})) \quad (11)$$

In a pseudo-potential approach \hat{V}_{ext} is replaced for each atom μ by a pseudo-potential \hat{V}_{ps} . The terms $\hat{V}_H[n]$ and $\hat{V}_{\text{xc}}[n]$ are local potentials and explicitly density dependent. Thus, the Hamiltonian $\hat{H}[n]$ and the wavefunctions $\psi_i([n], \mathbf{r})$ are also dependent on the electron density $n(\mathbf{r})$. Together with the expression Eq.(1) a self-consistency problem to obtain the charge density $n(\mathbf{r})$ is established, which is solved iteratively until the input density (used to define the potential terms in the Hamiltonian) is equal to the output density within the required accuracy. The number of self-consistency iterations N_{iter} is considerably reduced applying quasi-Newton methods⁵⁶.

The external potential $\hat{V}_{\text{ext}}[\{\mathbf{R}\}]$ depends explicitly on the positions $\{\mathbf{R}\}$ of all atoms, which change at certain steps to optimize the atomic structure or every time-step of a molecular dynamics algorithm. Thus, the Hamiltonian $\hat{H}[\{\mathbf{R}\}]$ and the wavefunctions $\psi_i(\{\mathbf{R}\}, r)$ are also dependent on the atomic positions $\{\mathbf{R}\}$. After the self-consistency condition for the electron density has been fulfilled, the atom positions are moved by a molecular static or molecular dynamics time-step, $\{\mathbf{R}(t)\} \rightarrow \{\mathbf{R}(t+\Delta t)\}$. Thus, for N_{MD} molecular time steps the eigenvalue problem has to be solved $N_{\text{MD}} N_{\text{iter}}$ times. These arguments suggest a particular loop structure of a typical first-principles method and a particular sequence how the different elements are calculated. This is summarized in Fig. 2.

Typical codes use LDA exchange correlation potentials and energies of Hedin and Lundqvist⁵⁷ or Vosko, Wilk, and Nusair⁵⁸, or GGA functionals of Perdew *et al.*^{59,60} are given as analytical expressions of the density and their derivatives in case of the GGA.

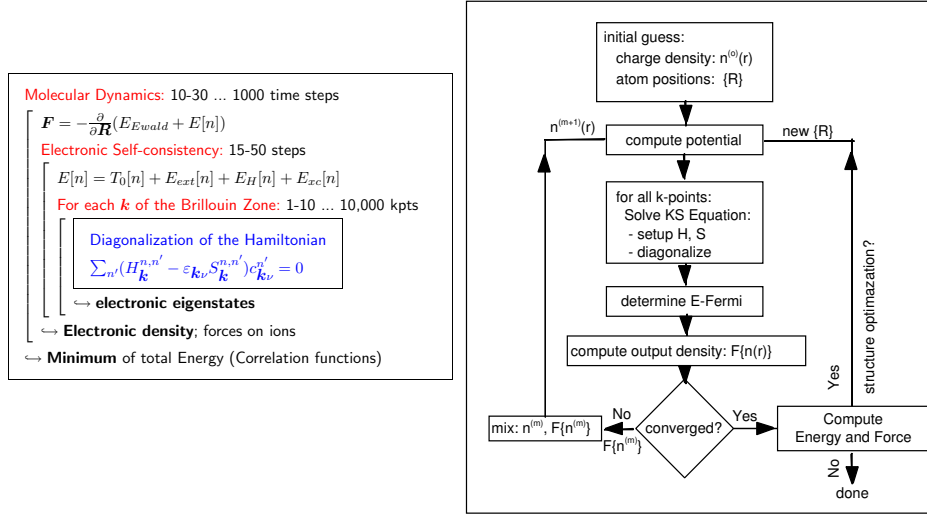


Figure 2. Right: Typical loop structure of a first-principles code based on density functional theory as applied solid state materials. Left: Schematic flow-chart for self-consistent density-functional calculations e.g. as realized by a FLAPW calculation.

2.3 Magnetism

If magnetism occurs, the ground state has a broken symmetry and the ground-state energy is described by functionals which depend on the vector-magnetization density $\mathbf{m}(\mathbf{r})$ as an additional field to the ordinary charge density $n(\mathbf{r})$, discussed so far. An additional term $\mu_B \underline{\sigma} \cdot \mathbf{B}_{xc}(\mathbf{r})$ appears in the Kohn-Sham equations Eq.(7), where $\mu_B = \frac{e\hbar}{2mc}$ is the Bohr magneton, \mathbf{B}_{xc} is the magnetic xc-field an electron experiences, and $\underline{\sigma}$ are the Pauli spinors. Thus, calculating magnetic systems, one works in a two-dimensional spin-space and the basis functions $\psi_{i\sigma}$ carry an additional spin label $\sigma = \pm 1$. The Hamiltonian is a 2×2 matrix in spin-space and is now hermitian and not symmetric. Complex magnetic structures lower frequently the symmetry of the problem and more states have to be calculated or a much larger fraction of the BZ (see Sect.2.6) has to be sampled, respectively, pushing the computational effort to the limits of modern supercomputers. In case of collinear magnetism, e.g. ferro-, ferri-, or antiferromagnetism, $\underline{\sigma} \cdot \mathbf{B}_{xc}$ reduces to $\underline{\sigma}_z \cdot B_{xc}$, the Hamiltonian is diagonal in spin space, the magnetization density m_z is then given by spin-up and -down densities, $m_z(\mathbf{r}) = n_{\uparrow}(\mathbf{r}) - n_{\downarrow}(\mathbf{r})$, and the effort of a magnetic calculation is just twice that of a nonmagnetic one. In general, the magnetic moment $\mathbf{M} = \int d\mathbf{r} \mathbf{m}(\mathbf{r})$ is a vector quantity, and the search of the magnetic structure can be done dynamically bearing similarities to the dynamical structure optimization combining molecular dynamics and simulated annealing. Therefore, everything said in this chapter on structural optimization applies to both, the atomic and the magnetic structure. Throughout the paper, the spin label is dropped for convenience. More information on the treatment of magnetism can be found in the chapter “Non-collinear magnetism: exchange parameter and T_C ” by G. Bihlmayer.

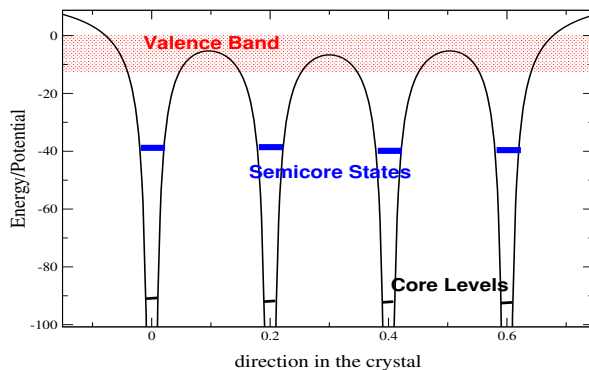


Figure 3. Schematic representation of the energy position of valence, semi-core and core electrons in periodic potential.

2.4 The Eigenvalue Problem

In all-electron methods eigenvalue problem Eq.(7) is solved for all occupied states i but typically subject to different boundary conditions. As shown schematically in Fig. 3 we distinguish core electrons from valence electrons. The former have eigenenergies which are at least a couple of Rydbergs below the Fermi energy, the potential they experience is to an excellent approximation spherically symmetric and the wavefunctions have no overlap to neighboring atoms. The eigenvalue problem of these states are solved applying the boundary conditions of isolated atoms, which is numerically tackled by a shooting method. Valence electrons in a crystalline solid form electron bands and the eigenvalue problem of is solved subject to the Bloch boundary conditions. The eigenstate is classified by the band index ν and a three-dimensional Bloch vector \mathbf{k} within the first Brillouin zone, ($i \in \{\mathbf{k}\nu\}$). Some materials contain chemical elements with states (e.g. $5p$ states of $4f$ elements or W, p states of early transition metals) intermediate between band and core states and those are coined semi-core states. These are high-lying and extended core states and particular care has to be taken on their treatment since their treatment as core states can cause significant errors in total energy, force and phonon calculations. According to the different treatment of the electrons, we decompose the charge density in the valence, semi-core and core densities

$$n(\mathbf{r}) = n_{\text{val}}(\mathbf{r}) + n_{\text{sc}}(\mathbf{r}) + n_{\text{core}}(r), \quad (12)$$

the latter being spherically symmetric. The charge densities are calculated according to Eq.(1). Wavefunctions and energies of core states give access to hyperfine quantities such as isomer shifts, hyperfine fields and electric field gradient as well as chemical shifts of core levels.

There are many possible ways to solve the Kohn-Sham equations for valence electrons. Frequently, a variational method is chosen by which a wavefunction $\psi_{\mathbf{k}\nu}(\mathbf{r})$ of Bloch vector \mathbf{k} and band index ν is sought as a linear combination of basis functions $\varphi_n(\mathbf{k}, \mathbf{r})$

$$\psi_{\mathbf{k}\nu}(\mathbf{r}) = \sum_{n=1}^N c_{\mathbf{k}\nu}^n \varphi_n(\mathbf{k}, \mathbf{r}) \quad (13)$$

satisfying the Bloch boundary conditions. $c_{\mathbf{k}\nu}^n$ are the expansion coefficients of the wavefunction (coefficient vector), and N is the number of basis functions taken into account. By this expansion, the eigenvalue problem

$$\hat{H}\psi_{\mathbf{k}\nu}(\mathbf{r}) = \varepsilon_{\mathbf{k}\nu}\psi_{\mathbf{k}\nu}(\mathbf{r}) \quad (14)$$

is translated in into an algebraic eigenvalue problem of dimension N

$$(\mathbf{H}(\mathbf{k}) - \varepsilon_{\mathbf{k}\nu}\mathbf{S}(\mathbf{k}))\mathbf{c}_{\mathbf{k}\nu} = 0 \quad \forall \mathbf{k} \in \text{BZ} \quad (15)$$

for the coefficient vector $c_{\mathbf{k}\nu}^n$ corresponding to the eigenvalues $\varepsilon_{\mathbf{k}\nu}$. The Hamilton $H^{n,n'}(\mathbf{k})$ and overlap matrices $S^{n,n'}(\mathbf{k})$ are hermitian or real symmetric, depending on the point symmetry of the atomic structure. If the basis functions are orthonormal, i.e. $\langle \varphi_n | \varphi_{n'} \rangle = \delta^{n,n'}$, as for example in case of simple planewaves, then the overlap matrix S , defined as

$$S^{n,n'}(\mathbf{k}) = \int_{\Omega} \varphi_n^*(\mathbf{k}, \mathbf{r}) \varphi_{n'}(\mathbf{k}, \mathbf{r}) d^3r \quad (16)$$

becomes diagonal, $S^{n,n'}(\mathbf{k}) = \delta^{n,n'}$, and the generalized eigenvalue problem Eq.(15) becomes of standard type. Ω is the volume of the unit cell.

In general, the general eigenvalue problem is reduced to a standard one using the Cholesky decomposition. It can be shown (e.g. Stoer⁶¹), that any hermitian and positive definite matrix can be decomposed into a matrix product of a lower triangular with only positive diagonal elements matrix and its transposed. Clearly, the overlap matrix satisfies these conditions and can be written $S = LL^{tr}$. Therefore, Eq.(15) becomes

$$\mathbf{H}\mathbf{c}_i = \varepsilon_i \mathbf{L}\mathbf{L}^{tr}\mathbf{c}_i, \quad (17)$$

multiplying from the left with L^{-1} and introducing a unit matrix we finally find

$$\mathbf{P}\mathbf{x}_i = \varepsilon_i \mathbf{x}_i, \quad (18)$$

after we have \mathbf{P} defined as $\mathbf{P} = L^{-1}\mathbf{H}(L^{-1})^{tr}$ and $\mathbf{x}_i = L^{tr}\mathbf{c}_i$. Thus, the generalized eigenvalue problem has been reduced to a simple one. The eigenvectors \mathbf{c}_i can be obtained by the back-transformation, $\mathbf{c}_i = (L^{tr})^{-1}\mathbf{x}_i$.

The choice of the most efficient numerical algorithm to solve Eq.(15) depends on the number of basis functions N and the number M of states ν taken into account. If $M/N > \sim 0.1$, direct numerical diagonalization schemes are employed, for example parallelized eigenvalue solver taken from the `SCALAPACK` library package. If $M/N < \sim 0.1$ or if N is too large to fit the eigenvalue problem into the memory of a computer the eigenvalue problem is solved iteratively. Any iterative solution of an eigenvalue problem can be divided into two parts: (i) the determination of the iterative improvement of the state vector $c_{\mathbf{k}\nu}^{n,[m]}$ at iteration step m by multiplying the Hamiltonian with the state vector to obtain the update $c_{\mathbf{k}\nu}^{n,[m+1]}$.

$$c_{\mathbf{k}\nu}^{n,[m+1]} = \sum_{n'} H^{n,n'}(\mathbf{k}) c_{\mathbf{k}\nu}^{n',[m]}, \quad (19)$$

and (ii) the orthonormalization of the wave functions

$$\sum_n c_{\mathbf{k}\nu}^{n,[m+1]} c_{\mathbf{k}\nu'}^{n,[m+1]} = \delta_{\nu,\nu'}. \quad (20)$$

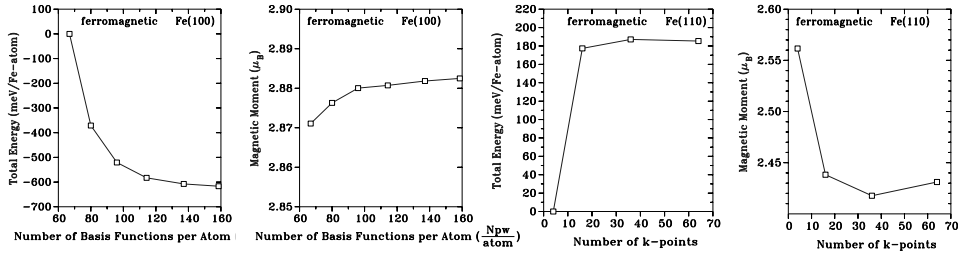


Figure 4. Test of convergence carried out by the FLAPW method of (absolute) total energy and magnetic moment as function (i) of the number of the LAPW basis functions (see two left figures) for a 7 layer Fe(100) film and (ii) number of special k-points in the IBZ (see two right figures) for an 11 layer Fe(110) film. The calculations of (i) were carried out for the $rk m$ -parameters $rk m = 7.5, 8.0, 8.5, 9.0, 9.5, 10.0$ corresponding to $N = 67, 80, 96, 114, 137, 158$ basis functions.

(iii) Frequently, each iteration step is accompanied by a direct sub-space diagonalization of a dimension proportional to M , on which Hamiltonian \hat{H} is projected. If the multiplication of $H \cdot c$ can be made fast by expressing the Hamiltonian in terms of dyadic products or convolutions as in norm-conserving or ultra-soft pseudo-potentials minimizing thereby the number of multiplications, iterative methods become particular beneficial.

2.5 The CPU Time Requirement

The number of basis functions N is determined by the required precision P of a calculation and by the volume Ω of the unit cell or the number of atoms in the unit cell, N_A , respectively. The precision P is controlled by the finest real-space resolution the basis functions can resolve. For three-dimensional unit cells N scales as $N \propto P^3$. In general, the triple $(N_{\mathbf{k}}, M, N)$, the number of k-vectors in the BZ used, the number M of states ν considered, and the number of basis functions N are determined by the required precision of the calculation and by the volume of the unit cell. These parameters determine the CPU-time and memory requirements of the calculations. Keeping the loop-structure in mind exhibited in Fig. 2, typically the calculational CPU time scales as

$$\text{CPU} \propto N_{\text{MD}} \cdot N_{\text{iter}} \cdot N_{\mathbf{k}} \begin{cases} N^3 & \text{direct diagonalization} \\ M_{\text{iter}}(MN \ln N + NM^2) & \text{iterative diagonalization} \end{cases} \quad (21)$$

where M_{iter} gives the number of eigenvalue iterations. This gives just a gross estimate as for iterative methods based on the Car-Parrinello idea where self-consistency iterations and eigenvalue iterations can be combined to directly minimize total energy functional $N_{\text{MD}} \cdot N_{\text{iter}} \cdot M_{\text{iter}}$ depends on many details. The scaling relation for precision scaling is:

$$\begin{aligned} \text{the number of k-points: } & N_{\mathbf{k}} \propto P_{\mathbf{k}}^3 & (22) \\ \text{the number of basis functions } N: & N \propto P^3, & (23) \end{aligned}$$

where $P_{\mathbf{k}}$ is the precision controlling the k-point summation, e.g. of the force, the total energy or the electron density. Assuming that the volume Ω of the unit cell is proportional

to the number of atoms N_A , the scaling relation for volume scaling is:

$$\text{the number of } \mathbf{k}\text{-points: } N_{\mathbf{k}} \propto 1/N_A, \quad (24)$$

$$\text{the number of states } \nu: M \propto N_A, \quad (25)$$

$$\text{the number of basis functions } N: N \propto N_A, \quad (26)$$

From these considerations it is argued to develop electronic structure methods (see Sect. 2.8) with efficient basis sets to reduce their number N , to develop algorithms to accelerate the convergence (see Sect. 2.7) and to employ an efficient \mathbf{k} -point integration scheme (see Sect. 2.6).

2.6 Brillouin-Zone Integration and Fermi Energy

The calculation of the electron density, total energy, force or stress tensor for infinite periodic solids require the integration of functions over the Brillouin zone that depend on the Bloch vector and the energy band. These integrations stretch only over the occupied part of the band, i.e. over the region of the Brillouin zone where the band energy $\epsilon_\nu(\mathbf{k})$ (ν is the band index) is lower than the Fermi energy. Hence, the integrals are of the form

$$\frac{1}{V_{BZ}} \int_{BZ} \sum_{\nu, \epsilon_\nu(\mathbf{k}) < E_F} f_\nu(\mathbf{k}) d^3k, \quad (27)$$

where f is the function to be integrated, e.g. $f = 1$ for the total number of electrons, $f = \epsilon$ for the eigenvalue sum and so on. Numerically, these integrations are performed on a discrete mesh in the Brillouin zone. In fact the effort of the BZ integration is in practice significantly reduced by employing the point group symmetry, where the integration is reduced to the irreducible wedge of the BZ (IBZ). There are different methods, that can be used to perform the integration, e.g. the special points method^{62,63} and the tetrahedron method⁶⁴⁻⁶⁶. The special points method is a method to integrate smoothly varying periodic functions of \mathbf{k} . The function to be integrated has to be calculated at a set of special points in the IBZ, each of which is assigned a weight. Thus, the BZ integration is transformed into a sum over a set of \mathbf{k} -points. At each \mathbf{k} -point a sharp energy cut-off is introduced to include only those state in the summation whose energy is below the Fermi energy. Thus, the integrals become:

$$\frac{1}{V_{BZ}} \int_{BZ} \sum_{\nu, \epsilon_\nu(\mathbf{k}) < E_F} f_\nu(\mathbf{k}) d^3k \longrightarrow \sum_{\mathbf{k} \in \text{IBZ}} \sum_{\nu, \epsilon_\nu(\mathbf{k}) < E_F} f_\nu(\mathbf{k}) w(\mathbf{k}) \quad (28)$$

Alternatively, this integration can be viewed as an integration over the whole Brillouin zone, where the function to be integrated is given by a product of the function f with a step function that cuts out the region of the Brillouin zone, where the band energy is above the Fermi energy. Clearly, the resulting function does not satisfy the condition of being smoothly varying. Therefore, the special \mathbf{k} -points method does not converge very quickly, and rather many \mathbf{k} -points are needed to obtain accurate results. On the other hand this method is simple to implement, because the weights depend only on \mathbf{k} and the band energy (via the step function) at each \mathbf{k} -point. Another problem arises from this ‘‘sharp’’ differentiation between occupied and empty bands (parts of bands). Let’s consider a band that is very close to the Fermi energy at a certain \mathbf{k} -point. During the iterations the

energy of this band might rise above or drop below the Fermi energy. This leads to sudden changes in the charge density, which can slow down or even prevent the convergence of the density. These sudden changes are clearly a result of the discretization in momentum space. To avoid this problem, the sharp edges of the step function are smoothed, e.g. by introducing a so-called temperature broadening in the context of a the Fermi function $(e^{(\epsilon-E_F)/k_B T} + 1)^{-1}$ rather than the step function. The temperature T or energy Tk_B are an additional external parameters adjusted to obtain the best convergence.

2.7 Achieving Self-Consistency

According to Sect. 2.2 the Kohn-Sham equation Eq.(7) are Schrödinger-like independent-particle equations which must be solved subject to the condition that the effective potential field $V_{\text{eff}}(\mathbf{r}) = V_{\text{ext}}(\mathbf{r}) + V_{\text{H}}(\mathbf{r}) + V_{\text{xc}}(\mathbf{r})$ and the density field $n(\mathbf{r})$ are consistent. The electron density $n_0(\mathbf{r})$ that minimizes the energy functional is a fix-point of the mapping

$$n'(\mathbf{r}) = F\{n(\mathbf{r})\}. \quad (29)$$

i.e. it solves

$$\mathcal{F}\{n_0(\mathbf{r})\} = 0, \quad \text{with } \mathcal{F}\{n(\mathbf{r})\} = F\{n(\mathbf{r})\} - n(\mathbf{r}). \quad (30)$$

(The same can be formulated for the potential.) Typically, the density is expanded into a large set of basis functions. Thus, in actual calculations, the charge density is a coefficient vector of dimension $N_{\text{Q}} \sim 8 * N$ (N defined as in Eq.(13) and Eq.(30) constitutes a system of N_{Q} nonlinear equations, which can be solved by iteration:

$$n^{m+1}(\mathbf{r}) = F\{n^m(\mathbf{r})\}. \quad (31)$$

A starting density $n^{(0)}(\mathbf{r})$ can be constructed by a superposition of atomic densities. A straight mapping as is suggested in Eq.(31) is in general divergent. Convergence can be achieved if the output density $F\{n^m(\mathbf{r})\}$ is mixed with the input density $n^m(\mathbf{r})$.

The simplest and slowest of such mixing schemes is the so-called “simple mixing”, which converges only linearly. The density for the next iteration is constructed as a linear combination of $n^{(m)}$ and $F\{n^{(m)}\}$ according to:

$$n^{(m+1)} = (1 - \alpha)n^{(m)} + \alpha F\{n^{(m)}\} = n^{(m)} + \alpha \mathcal{F}\{n^{(m)}\}, \quad (32)$$

where α is the so-called mixing parameter. If it is chosen small enough, the iteration converges and is very stable. However, for the type of systems one is interested in, α is very small, requiring many hundreds of iterations. In spin-polarized calculations different mixing parameters can be used for the charge and the magnetization density. Usually, the spin mixing parameter can be chosen far larger than the parameter for the charge density.

In the Newton-Raphson method, the functional $\mathcal{F}\{n\}$ is linearized around the approximate solution $n^{(m)}$.

$$\mathcal{F}\{n\} \approx \mathcal{F}\{n^{(m)}\} + \mathcal{J}\{n^{(m)}\}(n - n^{(m)}), \quad \mathcal{J}\{n^{(m)}(\mathbf{r})\} = \left. \frac{\partial \mathcal{F}\{n(\mathbf{r})\}}{\partial n(\mathbf{r}')} \right|_{n^{(m)}(\mathbf{r})}. \quad (33)$$

In actual calculations the Jacobian \mathcal{J} is a $N_{\text{Q}} \times N_{\text{Q}}$ matrix. Similar to the well-known Newton method to find zeros of one-dimensional functions, the next approximation to

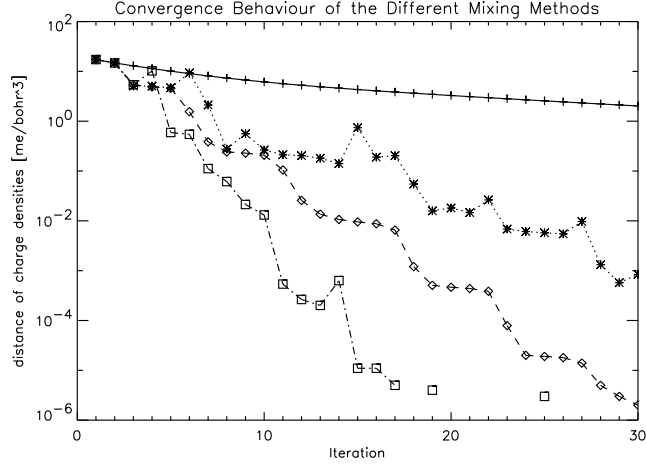


Figure 5. Comparison of the convergence of charge density calculated by different methods for a non-magnetic bcc Fe crystal using the FLAPW method. Calculations are carried out for mixing parameter $\alpha = 0.04$. + corresponds to simple mixing, and different quasi-Newton methods: * Broyden's 1st method, \diamond Broyden's 2nd method, \square generalized Anderson method. The distance of the residual vector vs. number of iterations is plotted semi-logarithmically⁶⁷.

$n_0, n^{(m+1)}$, is determined from the requirement, that the linearized functional in Eq.(33) vanishes at $n^{(m+1)}$. Thus, $n^{(m+1)}$ is given by:

$$n^{(m+1)} = n^{(m)} - \left[\mathcal{J}\{n^{(m)}\} \right]^{-1} \mathcal{F}\{n^{(m)}\}. \quad (34)$$

In opposite to the simple mixing, the Newton-Raphson method converges quadratically. The major drawback of this method is the difficulty to evaluate the Jacobian. Even if the functional $\mathcal{F}\{n\}$ were known, the evaluation would be cumbersome due to the enormous size of $\mathcal{J}\{n\}$. In addition, the Jacobian has to be inverted where the amount of calculation scales with cube of the dimension. A further problem is that the convergence radius is rather small so that the method can only be used if $n^{(m)}$ is already very close to n_0 .

The development of the Quasi-Newton methods made it possible to exploit the advantages of the Newton-Raphson method, i.e. to make use of the information that is contained in the Jacobian, for problems where the Jacobian cannot be calculated or its determination is too demanding. Rather than computing the Jacobian each iteration, an approximate Jacobian is set up and improved iteration by iteration. From the linearization of $\mathcal{F}\{n\}$ in Eq.(33) we find the following condition for the Jacobian, which is usually called Quasi-Newton condition:

$$\Delta n^{(m)} = \left[\mathcal{J}^{(m)} \right]^{-1} \Delta \mathcal{F}^{(m)} \quad (35)$$

$$\Delta n^{(m)} = n^{(m)} - n^{(m-1)}, \quad \Delta \mathcal{F}^{(m)} = \mathcal{F}\{n^{(m)}\} - \mathcal{F}\{n^{(m-1)}\}$$

Quasi-Newton methods converge super-linearly and have a larger convergence radius than the Newton-Raphson method. Since the Jacobian is build up iteration by iteration, the "his-

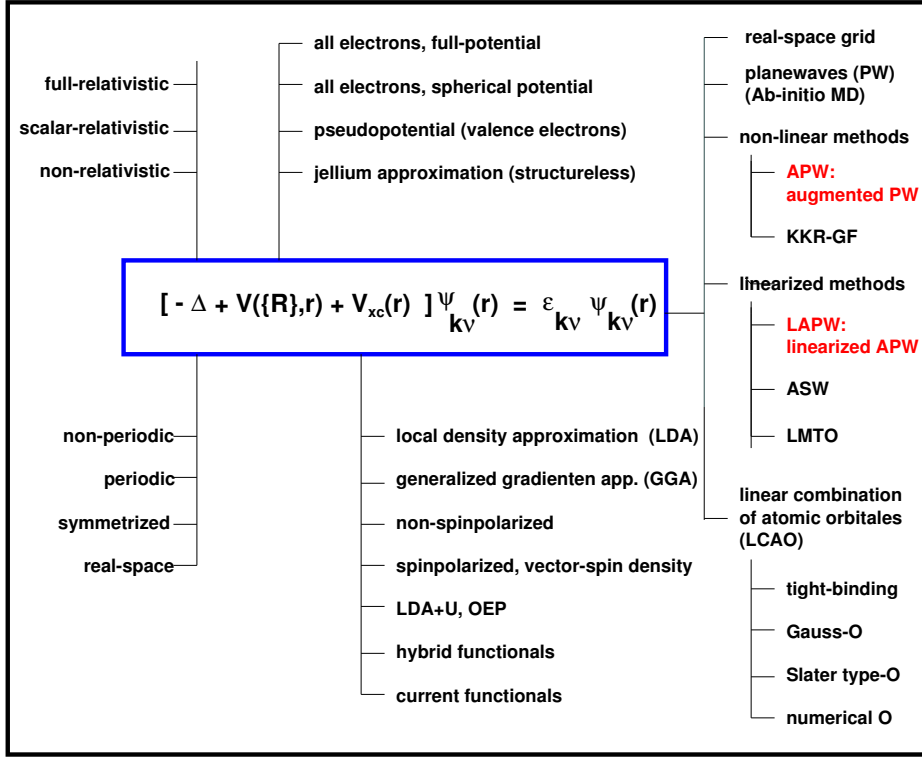


Figure 6. Very rough and schematic overview of electronic structure methods indicating a rich spectrum of methods developed for different purposes, applications, geometries and symmetries, chemical elements and materials requiring different approximations.

tory” of the previous iterations is memorized in \mathcal{J} , whereas the Jacobian of the Newton-Raphson method depends only on the previous iteration. In this sense the Newton-Raphson method is self-corrective³⁹, it “forgets” inadequately chosen corrections. The Quasi-Newton methods sometimes need to be restarted, if the iteration converges only slowly. This can happen if the starting density is very far from n_0 or when physical or numerical parameters that affect the calculations are changed during the iteration. Eq.(35) does not determine the Jacobian uniquely, instead Eq.(35) constitutes a system of N_Q equations for N_Q^2 unknowns. The various Quasi-Newton schemes differ by the ansatz how the new information is used to build the inverse Jacobian. The quality of the convergence is measured by the distance of the residual vector:

$$d_{n^{(m)}} = \|\mathcal{F}\{n^{(m)}\}\| = \|F\{n^{(m)}\} - n^{(m)}\|. \quad (36)$$

2.8 The Electronic Structure Methods

The quest to solve the Kohn-Sham equation (7) efficiently for periodic solids, solids with surfaces and interfaces, clusters and molecules has lead to a wide spectrum of very successful and efficient electronic structure methods. Treating isolated clusters or molecules,

methods based on localized orbitals are frequently selected going hand in hand with the chemical intuition of system in question. Considering methods applicable to periodic solids, frequently algorithms are chosen where the Bloch boundary condition can be included in the basis set. Guiding principles to develop electronic structure methods are by obtained by having a closer look at the mathematical nature of the Schrödinger-like Kohn-Sham equation Eq.(7) with the kinetic energy operator Δ and the $1/r$ singularity at the nucleus with the simultaneous necessity to calculate the xc-potential $V_{xc}[n](\mathbf{r})$ and the Hartree potential $V_H[n](\mathbf{r})$.

The planewave basis is obviously a very good choice, as the planewave is diagonal to the Laplace operator Δ appearing in both the the kinetic energy operator and in the Poisson equation to calculate the Hartree potential (see Eq.(8)), and for a function expanded in planewaves, its power is also completely expressible by a planewave expansion. This property is needed for calculating the charge density from the wave function. Thus, using a planewave basis set the calculation of the kinetic energy, charge density and the Hartree potential are obtained by simple algebraic expressions. The calculation of the $V_{xc}(\mathbf{r})$ best performed if the charge density is expressed in real-space. The discrete fast Fourier transformation (FFT) provides a fast algorithm to communicate between both spaces. However, planewave basis sets do not converge at the presence of the $1/r$ singularity. Thus, planewave basis-sets can only be used in the context of a pseudopotential approximation to the true potential where the $1/r$ potential has been replaced by an appropriate smooth potential.

All-electron methods have to cope with the $1/r$ singularity. Since this singularity cannot be dealt with variationally, one typically, works here with basis functions, which are the numerical solution of $(-\Delta + V_{\text{eff}} - E_l)\varphi = 0$ of the effective (spherical) potential containing the $1/r$ singularity, computed in a sphere around the atom at a given energy parameter E_l . These basis functions treat the singularity exactly. The matching of this wavefunction in such a sphere to the rest of the crystal outside the sphere divides the all-electron methods with regard to the eigenvalue dependence of the basis set into two groups: The nonlinear methods as for example the Korringa-Kohn-Rostocker (KKR) method (see chapter on KKR-Green-function method by Ph. Mavropoulos) and the APW method, and the linear methods, of which the most commonly used are the linear muffin-tin orbital method (LMTO)¹⁹, the augmented spherical⁶⁸ and the APW-based schemes, e.g. FLAPW method.

3 APW-like Concepts to solve the Kohn-Sham Equations

3.1 The APW Concept

There are many possible ways to solve the Kohn-Sham equations. Frequently, a variational method is chosen by which a wavefunction $\psi_{\mathbf{k},\nu}(\mathbf{r})$ of Bloch vector \mathbf{k} and band index ν is sought as a linear combination of basis functions $\varphi(\mathbf{r})$ satisfying the Bloch boundary conditions. The most straightforward choice would be to expand the wavefunction into planewaves or Fourier series, respectively,

$$\psi(\mathbf{k}, \nu) = \sum_{|\mathbf{k}+\mathbf{G}|\leq K_{\text{max}}} c_{\mathbf{k},\nu}^{\mathbf{G}} \exp[i(\mathbf{k} + \mathbf{G})\mathbf{r}]. \quad (37)$$

Here \mathbf{G} are all reciprocal lattice vectors up to the largest value of K_{max} and $c_{\mathbf{k},\nu}^{\mathbf{G}}$ are variational coefficients. The planewave basis set has some important advantages:

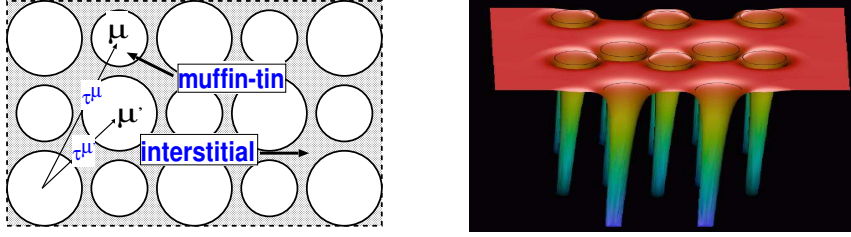


Figure 7. Left figure: Volume of unit cell partitioned into muffin-tin spheres of two different types of atoms and the interstitial region. Right figure: Actual self-consistent effective potential as obtained from an FLAPW calculation.

Planewaves are orthogonal, they are diagonal in momentum space and the implementation of planewave based methods is rather straightforward due to their simplicity. The credit goes to Slater¹⁵ having realized that owing to the singularity of the crystal potential at the nucleus, electron wavefunctions are varying very quickly near it, the planewave expansion would converge very slowly, large wavevectors (K_{\max}) would be needed to represent the wavefunctions accurately, which makes the set-up and diagonalization of the Hamiltonian matrix in terms of planewaves impracticable if not impossible. Even with the modern computer hardware, the planewaves are used only in the context of pseudopotential which allow an accurate description of the wavefunctions between the atoms, but avoid the fast oscillations near the core. Thus, less basis functions are needed.

In the APW method the space is partitioned into spheres centered at each atom site, the so-called muffin-tins (MTs), and into the remaining interstitial region (cf. Fig. 7). The MT spheres do not overlap and they are typically chosen such that they nearly (to allow for structural relaxations) fill the maximal possible space. Inside the muffin-tins, the potential is approximated to be spherically symmetric, and in many implementations the interstitial potential is set constant. The restrictions to the potential are commonly called shape-approximations. Noting that planewaves solve the Schrödinger equation in a constant potential, Slater suggested to replace the Bessel functions $j_l(Kr)$ in the Rayleigh decomposition of the planewave inside the sphere by radial functions $u_l(K, r)$, which match the Bessel functions in value at the sphere radius R_{MT} and whose product with the spherical harmonics $Y_L(\hat{\mathbf{r}})$ are the solutions in a spherical potential. It is this procedure what is understood by the term augmentation. Thus, the single wavefunctions $\psi_{\mathbf{k}, \nu}(\mathbf{r})$ are expressed as trial functions

$$\psi_{\mathbf{k}, \nu}(\mathbf{r}) = \sum_{|\mathbf{G}+\mathbf{k}| \leq K_{\max}} c_{\mathbf{k}, \nu}^{\mathbf{G}} \varphi_{\mathbf{G}}(\mathbf{k}, \mathbf{r}) \quad (38)$$

in terms of the APW basis functions:

$$\varphi_{\mathbf{G}}(\mathbf{k}, \mathbf{r}) = \begin{cases} e^{i(\mathbf{k}+\mathbf{G})\mathbf{r}} & \text{interstitial region} \\ \sum_{lm} a_L^{\mu \mathbf{G}}(\mathbf{k}) u_l(r^\mu | E) Y_L(\hat{\mathbf{r}}^\mu) & \text{muffin-tin } \mu \end{cases} \quad (39)$$

The position \mathbf{r} inside the spheres μ located at $\boldsymbol{\tau}^\mu$ (see Fig. 7) is given with respect to the center of each sphere. L abbreviates the quantum numbers l and m and u_l is the regular

solution of the radial Schrödinger equation

$$\left\{ -\frac{\hbar^2}{2m} \frac{\partial^2}{\partial r^2} + \frac{\hbar^2}{2m} \frac{l(l+1)}{r^2} + V(r) - E \right\} r u_l(r) = 0 \quad (40)$$

to the energy parameter E_l . Here, $V(r)$ is the spherical component of the potential $V(\mathbf{r})$. The coefficients

$$a_L^{\mu\mathbf{G}}(\mathbf{k}) = a_L^\mu(\mathbf{k} + \mathbf{G}) = 4\pi \exp(i\mathbf{k}\boldsymbol{\tau}^\mu) i^l Y_L^*(\hat{\mathbf{K}}) \frac{j_l(KR^\mu)}{u_l(R^\mu)}, \quad \mathbf{K} = \mathbf{k} + \mathbf{G} \quad (41)$$

are determined from the requirement, that the wavefunctions are continuous at the boundary of the muffin-tin spheres in order for the kinetic energy to be well-defined. The variational coefficients $c^{\mathbf{G}}$ uniquely determine the wavefunction in the interstitial region.

If E were kept fixed, used only as a parameter during the construction of the basis, the Hamiltonian could be set up in terms of this basis. This would lead to a standard secular equation for the band energies where for a given \mathbf{k} -point in the Brillouin zone (BZ) a set of band energies E_ν are determined. Unfortunately, it turns out, that the APW basis does not offer enough variational freedom if E is kept fixed. An accurate description can only be achieved if the energies are set to the corresponding band energies $E_{\mathbf{k},\nu}$. In this case the Hamiltonian matrix H depends not only on \mathbf{k} , $H(\mathbf{k})$, but also on $E_{\mathbf{k},\nu}$, $H(E_{\mathbf{k},\nu})$, and the latter can no longer be determined by a simple diagonalization. Since the u_l 's depend then on the band energies, the solution of the secular equation becomes a nonlinear problem, which is computationally much more demanding than a secular problem. One way of solving this problem is to fix the energy E and scan over \mathbf{k} to find a solution, i.e. find one band at the time, instead of diagonalizing a matrix to find all the bands at a given \mathbf{k} . Thus, in Slater's formulation of the method E enters as an additional non-linear variational parameter varying the shape of the functions u_l till the optimal shape is found for the band energies $E_{\mathbf{k},\nu}$ one has looked for. There are several other limitations connected to the APW method. One is rather obvious, when $u_l(R)$ in Eq.(41) becomes zero at the MT boundary, the radial function and the planewave becomes decoupled, known as the asymptote problem. Others are beyond the scope of the chapter. Further information about the APW method can be found in the book by Loucks¹⁷, which also reprints several early papers including Slater's original publication¹⁵.

There is one remaining point. Please notice that the APW method produces per construction principle wavefunctions with a discontinuity in the slope at the muffin-tin boundary. Due to these discontinuous first derivatives the secular equation in the APW basis

$$\sum_{\mathbf{G}'} (\langle \varphi_{\mathbf{G}} | H - \varepsilon_{\mathbf{k}\nu} | \varphi_{\mathbf{G}'} \rangle + \langle \varphi_{\mathbf{G}} | T_S | \varphi_{\mathbf{G}'} \rangle) c_{\mathbf{k}\nu}^{\mathbf{G}'} = 0 \quad (42)$$

contains a second term due to the matrix elements $\langle \psi | -\nabla^2 | \psi \rangle$ of the kinetic energy operator T commonly defined as $T = -\nabla^2$, which is replaced by $\langle \nabla\psi | \nabla\psi \rangle$, leading then via Green's theorem to the appearance of additional surface integrals $T_S \propto \int \psi^* \left[\left(\frac{\partial\psi}{\partial n} \right)_- - \left(\frac{\partial\psi}{\partial n} \right)_+ \right] dS$, where $+(-)$ indicates just outside and inside the muffin-tin sphere. The matrix elements of T_S are proportional to the difference of the logarithmic derivatives from the function u_l , $D(u_l|E) = \frac{u_l'(R)}{u_l(R)}$, and that of an empty sphere $D(j_l|E) = \frac{j_l'(R)}{j_l(R)}$, taken at the sphere boundary. The logarithmic derivatives are related to

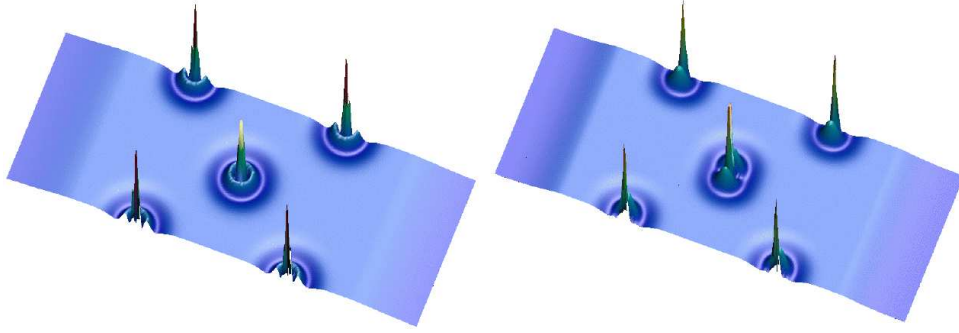


Figure 8. Square of the LAPW basisfunction generated for $\mathbf{G} = 0$ and \mathbf{k} at the origin ($\bar{\Gamma}$ -point) (left) and boundary (\bar{M} -point) (right) of the Brillouin zone of a 3-layer thin film of Cu(100). The cuts are taken in the $\{110\}$ plane. The basisfunctions are optimally suited to represent $4s$ states of Cu (left) and $4p$ states (right).

the phase shifts in scattering events. Thus, the second term in Eq.(42) can be interpreted describing the scattering of a planewave coming from the crystal at the sphere of the atoms. It is well-known that the logarithmic derivatives and the phase shifts are energy dependent quantities, which explains the explicit energy dependence of the APW Hamiltonian in particular, and all nonlinear electronic structure methods in general.

3.2 The LAPW Basisfunctions

To avoid the problems connected with the APW method resulting from the energy dependence of the Hamiltonian, in the middle of the seventies linearized methods were invented by Andersen¹⁹ and Koelling and Arbmán²⁰. Based on an idea proposed by Marcus²², the basis functions u_l in the muffin-tins were supplemented by their energy derivatives \dot{u}_l , but both, u_l and \dot{u}_l , are now evaluated at a fixed energy E_l . The original energy dependence of the radial basis-function is thereby replaced by the Taylor series:

$$u_l(E) = u_l(E_l) + (E - E_l)\dot{u}_l(E_l) + \dots \quad (43)$$

terminated after the linear term. In this way, the wavefunctions are affected by an error which is quadratic in the deviation of the eigenvalue E from the energy parameter E_l , the error in the eigenvalues enter only to fourth order²⁰. With this extension, the explicit form of the basis functions is now:

$$\psi_{\mathbf{G}}(\mathbf{k}) = \begin{cases} \exp(i(\mathbf{k} + \mathbf{G})\mathbf{r}) & \text{interstitial} \\ \sum_{l,m} (a_{lm}^{\mu,\mathbf{G}}(\mathbf{k})u_l^\mu(r) + b_{lm}^{\mu,\mathbf{G}}(\mathbf{k})\dot{u}_l^\mu(r))Y_{lm}(\hat{\mathbf{r}}^\mu) & \text{muffin-tin } \mu. \end{cases} \quad (44)$$

Examples of LAPW basisfunctions are shown in Fig. 8. The values of the coefficients $a_{lm}^{\mu,\mathbf{G}}(\mathbf{k})$ and $b_{lm}^{\mu,\mathbf{G}}(\mathbf{k})$ are determined to ensure continuity in value and derivative of the basis functions across the muffin-tin boundary. (A detailed description of these coefficients will follow in Sect. 4.2.3.) Thereby, also the surface integrals $\int \psi^* \left(\frac{\partial \psi}{\partial n} \right) dS$ which were encountered in the APW method disappear. In this way, the energy dependence of the

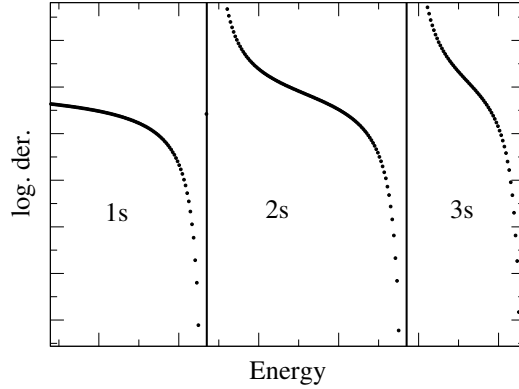


Figure 9. Schematic drawing of the logarithmic derivative, $\frac{u_l'(R)}{u_l(R)}$, for $l = 0$ as function of the energy. The asymptotes indicate where the nodes of the wavefunction pass through the muffin-tin radius. They separate the branches labeled 1s, 2s and 3s.

Hamiltonian is removed, simplifying the eigenvalue problem, Eq.(15), to a standard problem of linear algebra. Instead of working with u_l and \dot{u}_l several LAPW implementations follow the ASW idea, working only with u_l but for two different energy parameters E_l and E_l' . As we see below working with u_l and \dot{u}_l is rather elegant.

If \hat{H}_{sp}^μ denotes the spherical Hamiltonian in Eq.(40), \dot{u} can be determined from the energy derivative of this equation at E_l :

$$\hat{H}_{sp}^\mu \dot{u}_l^\mu = E_l \dot{u}_l^\mu + u_l^\mu. \quad (45)$$

The normalization of the radial functions is usually chosen like: ^a

$$\int_0^{R^\mu} r^2 u_l^{\mu 2} dr = 1 \quad (46)$$

and the energy derivatives, \dot{u}_l^μ , are orthogonal to the radial functions, i.e.

$$\int_0^{R^\mu} r^2 u_l^\mu \dot{u}_l^\mu dr = 0 \quad (47)$$

a relation, which will simplify the calculation of the elements of the Hamilton matrix.

Stimulated by the idea of the LAPW basis set, one may ask to improve the basis set by matching only the 1st derivative continuously, but also higher derivatives working with higher energy derivatives of u_l . This approach has actually been followed by Takeda and Kübler⁶⁹ using n energy parameters to match the wavefunction continuously till the $(n - 1)$ st derivative. However, it turned out that such wavefunctions are variationally very stiff and the convergence of the results with respect of the number of basis functions is rather slow. This can be understood by following this procedure up to the extreme were the

^aIn the many LAPW-codes, the electrons in the muffin-tin are treated in the scalar-relativistic approximation³⁵. This means that a two-component wavefunction is used and the normalization conditions are modified accordingly. For the continuity conditions, only the “large component” of the radial function is taken into account. To keep the formalism as simple as possible, in the following we will discuss only the non-relativistic case.

wavefunction matches to all derivatives. Then we know, the u_l must be the Besselfunction j_l or the planewave, respectively. We have already argued before that this requires an infinite number of planewave to describe the wavefunction at the $1/r$ singularity. Thus, it is a great merit of the LAPW basis set, that the basis set is linear, but nearly as efficient as the APW method. The speed of convergence with respect to the number of basisfunctions can even be improved by the introduction of local orbitals (see Sect. 3.3).

The energies E_l are chosen to minimize the linearization errors, i.e. in the center of gravity of the l -like bands. It should be noticed here, that the choice of the energy parameter in a certain sense also determines the nodal structure of the wavefunction. A basis function, where the $l = 1$ energy parameter is chosen to describe a $2s$ -like wavefunction in a certain muffin-tin, will not be suitable to describe a $3s$ or a $1s$ state. The energy parameter is then said to be within the $2s$ branch (cf. Fig. 9). The flexibility of the basis function of course also depends on the size of the muffin-tin radius, R , so that with the choice of a smaller R in some cases two branches can be forced to “collapse” to a single branch⁷⁰. On the other hand, a smaller flexibility allows to separate core- from valence states in a calculation. Thus, in a typical calculation only high-lying valence states are calculated (e.g. $3s$, $3p$, $3d$), while very localized states (e.g. $1s$, $2s$, $2p$) are excluded from the calculation. These states are then treated in a separate, atomic like, calculation using the $l = 0$ part of the muffin-tin potential.

As a final point, we will address the question how large l should be in a realistic calculation. Since the a and b coefficients in Eq.(44) should ensure continuity across the muffin-tin boundary, the plane-wave cutoff, G_{\max} and the l cutoff, l_{\max} , are normally chosen to match: A plane-wave with wavevector G_{\max} (given in inverse atomic units) has G_{\max}/π nodes per atomic unit. A spherical harmonic with $l = l_{\max}$ has $2l_{\max}$ nodes along a great circle on the muffin-tin sphere, i.e. there are $l_{\max}/(\pi R)$ nodes per atomic unit. Therefore, a reasonable choice of the cutoffs is $l_{\max} = RG_{\max}$, typically $l_{\max} = 8$ is chosen.

3.3 Local Orbitals: LAPW+LO and APW+lo

In certain materials high-lying core states, the so-called semicore states, pose a problem to LAPW calculations: they are too delocalized to be described as core electrons (contained entirely in the muffin-tin), but the energy parameter E_l , which would be needed for their description, is already used to describe higher lying valence states. E.g. the $5p$ levels of La are too high in energy to be neglected in total energy calculations⁴³. Several possible strategies have been proposed to overcome this problem: The above mentioned reduction of the size of the muffin-tin radius⁷⁰, so-called two-window calculations⁷¹, and the use of local orbitals⁴³.

The local orbitals are an extension to the FLAPW basis, that can be used to improve the variational freedom for a specific purpose, e.g. to improve the representation of the semicore states. The extra basis functions are completely localized inside the muffin-tin spheres, i.e. their value and derivative falls to zero at the muffin-tin radius. Thus, no additional boundary conditions have to be satisfied. This can be achieved via a linear combination including three radial functions, the standard FLAPW functions u_l^μ and \dot{u}_l^μ plus a further radial function $u_{l_o}^\mu$. This new radial function is constructed in the same way as u_l^μ , but with a different energy parameter $E_{l_o}^\mu$. If the local orbitals are used to treat semicore states, this energy parameter is set to the energy of these states. The local orbitals can be

used very specifically, e.g. if they are applied to the 5p semicore states of tungsten only local orbitals with p -character are added to the basis.

The three functions u_l^μ , \dot{u}_l^μ and $u_{l_o}^\mu$ have to be combined, so that the value and the derivative of the local orbital go to zero at the muffin-tin radius. Additionally, the resulting radial functions can be required to be normalized. Hence, to determine the coefficients of the radial functions $\tilde{a}_{l_o}^\mu$, $\tilde{b}_{l_o}^\mu$ and $\tilde{c}_{l_o}^\mu$ we make use of the following three conditions:

$$\tilde{a}_{l_o}^\mu u_l^\mu(R^\mu) + \tilde{b}_{l_o}^\mu \dot{u}_l^\mu(R^\mu) + \tilde{c}_{l_o}^\mu u_{l_o}^\mu(R^\mu) = 0 \quad (48)$$

$$\tilde{a}_{l_o}^\mu \frac{\partial u_l^\mu}{\partial r}(R^\mu) + \tilde{b}_{l_o}^\mu \frac{\partial \dot{u}_l^\mu}{\partial r}(R^\mu) + \tilde{c}_{l_o}^\mu \frac{\partial u_{l_o}^\mu}{\partial r}(R^\mu) = 0 \quad (49)$$

$$\int_0^{R^\mu} (\tilde{a}_{l_o}^\mu u_l^\mu(R^\mu) + \tilde{b}_{l_o}^\mu \dot{u}_l^\mu(R^\mu) + \tilde{c}_{l_o}^\mu u_{l_o}^\mu(R^\mu))^2 r^2 dr = 1 \quad (50)$$

Where l_o is the index of the local orbital, which is necessary because more than one local orbital can be added for each atom. The local orbitals are finally coupled to “fictitious” planewaves, \mathbf{G}_{l_o} , in the same way as the FLAPW basis functions:

$$\varphi_{\mathbf{G}_{l_o}}^{\mu, l_o}(\mathbf{k}, \mathbf{r}) = \sum_m \left(a_{L_o}^{\mu, \mathbf{G}_{l_o}}(\mathbf{k}) u_l^\mu + b_{L_o}^{\mu, \mathbf{G}_{l_o}}(\mathbf{k}) \dot{u}_l^\mu + c_{L_o}^{\mu, \mathbf{G}_{l_o}}(\mathbf{k}) u_{l_o}^\mu \right) Y_L(\hat{\mathbf{r}}) \quad (51)$$

with

$$a_{L_o}^{\mu, \mathbf{G}_{l_o}}(\mathbf{k}) = e^{i(\mathbf{k} + \mathbf{G}_{l_o}) \cdot \mathbf{r}^\mu} \tilde{a}_{l_o}^\mu 4\pi \frac{1}{W} i^l Y_L^*(\mathbf{k} + \mathbf{G}_{l_o}) \quad (52)$$

and similarly for the b and c coefficients (cf. Eq.(79)).

It should be noted here that, although originally developed to treat semicore states, the LAPW+LO scheme allows also the treatment of higher lying states, that are far above the energy parameters E_l of conventional LAPW and which are impossible to describe with decent accuracy^b. Similar concepts have been explored by Krasovskii and Schattke^{72,73} in the extended LAPW method.

Another drawback of the linearized methods (as compared to the APW method) is the slower convergence of the results (e.g. eigenvalues) with respect to the number of basis functions that are used in the calculation. The condition of continuous first derivative at the muffin-tin boundary made the LAPW basis functions “stiffer” as compared to the APW’s. Although the LAPW’s are flexible in describing wavefunctions far from the linearization energy E_l , they provide a poorer basis close to E_l . This leads to an increasing number of LAPW’s, that have to be used to describe the wavefunction. An alternative way of linearizing the APW method has been proposed by Sjöstedt *et al.*⁴⁴: The APW basis functions (Eq.(39) but now evaluated at a fixed energy) are complemented within the muffin-tin by another type of local orbitals:

$$\varphi_{\mathbf{G}_{l_o}}^{\mu, l_o}(\mathbf{k}, \mathbf{r}) = \sum_m \left(a_{L_o}^{\mu, \mathbf{G}_{l_o}}(\mathbf{k}) u_l^\mu + b_{L_o}^{\mu, \mathbf{G}_{l_o}}(\mathbf{k}) \dot{u}_l^\mu \right) Y_L(\hat{\mathbf{r}}) \quad (53)$$

which are evaluated at the same energy as the the APW’s. The coefficients a and b are chosen such, that this local orbital vanishes at the muffin-tin boundary. This introduces

^bOf course accuracy refers here always to the linearization error in comparison to the APW method. Whether an accurate description of individual states, especially higher lying ones, is possible in DFT at all is not our concern here.

again a discontinuous first derivative at the muffin-tin radius, and the surface integral, that appeared in the APW method, has to be calculated. But in many cases this (small) additional numerical effort is compensated by a faster convergence with respect to the number of basis functions. Especially for structures with atoms with small muffin-tin radius (like O or N) this APW+lo method can lead to significant savings in computing time^{44,74}. The question, up to which l the APW's should be supplemented with these lo's without introducing too large computational costs and from which l on a normal (L)APW basis-set can be used without causing numerical errors has been investigated by Madsen *et al.*⁷⁴.

4 The FLAPW Method

4.1 The Concept of FLAPW

The full-potential LAPW method (FLAPW)^{24,12} combines the choice of the LAPW basis set with the treatment of the full-potential and charge density without any shape-approximations in the interstitial region and inside the muffin-tins. This generalization is achieved by relaxing the constant interstitial potential V_I^0 and the spherical muffin-tin approximation $V_{MT}^0(r)$ due to the inclusion of a warped interstitial $\sum V_I^{\mathbf{G}} e^{i\mathbf{G}\mathbf{r}}$ and the non-spherical terms inside the muffin-tin spheres:

$$V(\mathbf{r}) = \begin{cases} \sum_{\mathbf{G}} V_I^{\mathbf{G}} e^{i\mathbf{G}\mathbf{r}} & \text{interstitial region} \\ \sum_L V_{MT}^L(r) Y_L(\hat{\mathbf{r}}) & \text{muffin-tin} \end{cases} \quad (54)$$

This method became possible with the development of a technique for obtaining the Coulomb potential for a general periodic charge density without shape-approximations and with the inclusion of the Hamiltonian matrix elements due to the warped interstitial and non-spherical terms of the potential. The charge density n , is represented analogously to Eq.(54), just exchanging V by n . Details of the solution of the Poisson equation for an arbitrarily shaped periodic potential are described in Sect. 4.6.

4.2 Construction of the Hamiltonian Matrix

The FLAPW Hamiltonian and overlap matrices consist of two contributions from the two regions into which space is divided.

$$H = H_I + H_{MT} \quad \text{and} \quad S = S_I + S_{MT} \quad (55)$$

Both contributions have to be computed separately.

4.2.1 Contribution of the Muffin-Tins

Writing the product of the radial functions u with the spherical harmonics as $\phi_L = u_L Y_L$, the contribution of the muffin-tin to the Hamiltonian matrix and the overlap matrix is given

by:

$$H_{MT}^{\mathbf{G}'\mathbf{G}}(\mathbf{k}) = \sum_{\mu} \int_{MT\mu} \left(\sum_{L'} a_{L'}^{\mu\mathbf{G}'}(\mathbf{k}) \phi_{L'}^{\alpha}(\mathbf{r}) + b_{L'}^{\mu\mathbf{G}'}(\mathbf{k}) \dot{\phi}_{L'}^{\alpha}(\mathbf{r}) \right)^* \hat{H}_{MT\alpha} \left(\sum_L a_L^{\mu\mathbf{G}}(\mathbf{k}) \phi_L^{\alpha}(\mathbf{r}) + b_L^{\mu\mathbf{G}}(\mathbf{k}) \dot{\phi}_L^{\alpha}(\mathbf{r}) \right) d^3r \quad (56)$$

(The overlap matrix $S_{MT}^{\mathbf{G}'\mathbf{G}}(\mathbf{k})$ is obtained by replacing $\hat{H}_{MT\alpha}$ by 1.) It is distinguish between the atom index μ and the atom type index $\alpha(\mu)$. In most application they are symmetry equivalent atoms in the unit cell, i.e. some atoms can be mapped onto each other by space group operations. Clearly, these atoms must possess the same physical properties, e.g. the potential has to be equal. As a consequence, the Hamiltonian and the basis functions $\phi_L^{\alpha}(\mathbf{r})$ do not differ among the atoms of the same type. This fact is exploited in that the muffin-tin potential of an atom type is only stored once for the representative atom, and the matrices Eq.(58) is also calculated for the representative only. $\hat{H}_{MT\alpha}$ is the scalar relativistic Hamiltonian operator. It can be split up into two parts, the spherical Hamiltonian \hat{H}_{sp} (cf. Eq. (40)) and the nonspherical contributions to the potential V_{ns} .

$$\hat{H}_{MT\alpha} = \hat{H}_{sp}^{\alpha} + V_{ns}^{\alpha} \quad (57)$$

The above integrations contain the following type of matrix elements.

$$t_{L'L}^{\alpha\phi\phi} = \int_{MT\alpha} \phi_{L'}^{\alpha}(\mathbf{r}) \hat{H}_{MT\alpha} \phi_L^{\alpha}(\mathbf{r}) d^3r \quad (58)$$

These matrix elements do not depend on the $A_L^{\mu\mathbf{G}}(\mathbf{k})$ and $B_L^{\mu\mathbf{G}}(\mathbf{k})$ coefficients. Thus, they are independent of the Bloch vector and need to be calculated only once per iteration. The functions ϕ_L^{α} and $\dot{\phi}_L^{\alpha}$ have been constructed to diagonalize the spherical part \hat{H}_{sp}^{α} of the muffin-tin Hamiltonian $\hat{H}_{MT\alpha}$:

$$\hat{H}_{sp}^{\alpha} \phi_L^{\alpha} = E_l \phi_L^{\alpha} \quad \text{and} \quad \hat{H}_{sp}^{\alpha} \dot{\phi}_L^{\alpha} = E_l \dot{\phi}_L^{\alpha} + \phi_L^{\alpha}. \quad (59)$$

Multiplying these equations with $\phi_{L'}^{\alpha}(\mathbf{r})$ and $\dot{\phi}_{L'}^{\alpha}(\mathbf{r})$ respectively and integrating over the muffin-tins gives

$$\begin{aligned} \langle \phi_{L'}^{\alpha} | \hat{H}_{sp}^{\alpha} \phi_L^{\alpha} \rangle_{MT\alpha} &= \delta_{ll'} \delta_{mm'} E_l \quad ; \quad \langle \phi_{L'}^{\alpha} | \hat{H}_{sp}^{\alpha} \dot{\phi}_L^{\alpha} \rangle_{MT\alpha} = \delta_{ll'} \delta_{mm'} \\ \langle \dot{\phi}_{L'}^{\alpha} | \hat{H}_{sp}^{\alpha} \phi_L^{\alpha} \rangle_{MT\alpha} &= 0 \quad ; \quad \langle \dot{\phi}_{L'}^{\alpha} | \hat{H}_{sp}^{\alpha} \dot{\phi}_L^{\alpha} \rangle_{MT\alpha} = \delta_{ll'} \delta_{mm'} E_l \langle \dot{u}_l^{\alpha} | \dot{u}_l^{\alpha} \rangle_{MT\alpha} \end{aligned} \quad (60)$$

Where the normalization condition for u_l^{α} has been used. So, only the expectation values of the nonspherical part of the potential are left to be determined. Since the potential is also expanded into a product of radial functions and spherical harmonics,

$$V^{\alpha}(\mathbf{r}) = \sum_{L''} V_{L''}^{\alpha}(r) Y_{L''}(\hat{\mathbf{r}}), \quad (61)$$

the corresponding integrals consist of product of a radial integrals and angular integrals over three spherical harmonics, the so-called Gaunt coefficients:

$$t_{L'L}^{\alpha\phi\phi} = \sum_{l''} I_{l'l''}^{\alpha uu} G_{l'l''}^{m'm''} + \delta_{ll'} \delta_{mm'} E_l \quad (62)$$

with

$$G_{l'l''}^{mm'm''} = \int Y_{lm}^* Y_{l'm'} Y_{l''m''} d\Omega \quad \text{and} \quad I_{l'l''}^{\alpha u u} = \int u_l^\alpha(r) u_{l''}^\alpha(r) V_{l''}^\alpha(r) r^2 dr \quad (63)$$

as well as similar expressions for $I_{l'l''}^{\alpha u i}$ and others. The I matrices contain the radial integrals. Finally, the Hamiltonian and overlap matrix elements become

$$\begin{aligned} H_{MT}^{\mathbf{G}'\mathbf{G}}(\mathbf{k}) &= \sum_{\mu} \sum_{L'L} (a_{L'}^{\mu\mathbf{G}'}(\mathbf{k}))^* t_{L'L}^{\alpha\phi\phi} a_L^{\mu\mathbf{G}}(\mathbf{k}) + (b_{L'}^{\mu\mathbf{G}'}(\mathbf{k}))^* t_{L'L}^{\alpha\phi\phi} b_L^{\mu\mathbf{G}}(\mathbf{k}) \\ &\quad + (a_{L'}^{\mu\mathbf{G}'}(\mathbf{k}))^* t_{L'L}^{\alpha\phi\phi} b_L^{\mu\mathbf{G}}(\mathbf{k}) + (b_{L'}^{\mu\mathbf{G}'}(\mathbf{k}))^* t_{L'L}^{\alpha\phi\phi} a_L^{\mu\mathbf{G}}(\mathbf{k}) \end{aligned} \quad (64)$$

$$S_{MT}^{\mathbf{G}'\mathbf{G}}(\mathbf{k}) = \sum_{\mu} \sum_L (a_L^{\mu\mathbf{G}'}(\mathbf{k}))^* a_L^{\mu\mathbf{G}}(\mathbf{k}) + (b_L^{\mu\mathbf{G}'}(\mathbf{k}))^* b_L^{\mu\mathbf{G}}(\mathbf{k}) \langle \dot{u}_l^\alpha | \dot{u}_l^\alpha \rangle_{MT\mu} \quad (65)$$

4.2.2 The Interstitial Contribution

The interstitial contributions to the Hamiltonian and overlap matrix have the following form.

$$H_I^{\mathbf{G}'\mathbf{G}}(\mathbf{k}) = \frac{1}{\Omega} \int_I e^{-i(\mathbf{G}+\mathbf{k})\mathbf{r}} \left(-\frac{\hbar^2}{2m} \Delta + V(\mathbf{r}) \right) e^{i(\mathbf{G}'+\mathbf{k})\mathbf{r}} d^3r \quad (66)$$

$$S_I^{\mathbf{G}'\mathbf{G}} = \frac{1}{\Omega} \int_I e^{-i(\mathbf{G}+\mathbf{k})\mathbf{r}} e^{i(\mathbf{G}'+\mathbf{k})\mathbf{r}} d^3r \quad (67)$$

The potential is also expanded into planewaves in the interstitial region.

$$V(\mathbf{r}) = \sum_{\mathbf{G}'} V_{\mathbf{G}'} e^{-i\mathbf{G}'\mathbf{r}} \quad (68)$$

Without the existence of the muffin-tin spheres the integration would stretch over the entire unit cell and the integration becomes rather simple. The kinetic energy is diagonal in momentum space and the potential is local, diagonal in real space and of convolution form in momentum space.

$$H_I^{\mathbf{G}'\mathbf{G}}(\mathbf{k}) = \frac{\hbar^2}{2m} |\mathbf{G} + \mathbf{k}|^2 \delta_{\mathbf{G}\mathbf{G}'} + V_{(\mathbf{G}-\mathbf{G}')}$$

$$S_I^{\mathbf{G}'\mathbf{G}} = \delta_{\mathbf{G}\mathbf{G}'}$$

However, these matrix elements are not as straightforward to calculate as they appear at first glance, because of the complicated structure of the interstitial region. The integrations have to be performed only in between the muffin-tins. Therefore, a step function $\Theta(\mathbf{r})$ has to be introduced, that cuts out the muffin-tins.

$$\Theta(\mathbf{r}) = \begin{cases} 1 & \text{interstitial region} \\ 0 & \text{muffin-tins} \end{cases} \quad (69)$$

Using the step function the matrix elements can be written:

$$H_I^{\mathbf{G}\mathbf{G}'}(\mathbf{k}) = \frac{1}{\Omega} \int_{cell} e^{-i(\mathbf{G}-\mathbf{G}')\mathbf{r}} V(\mathbf{r})\Theta(\mathbf{r})d^3r + \frac{1}{2}(\mathbf{G}' + \mathbf{k})^2 \frac{1}{\Omega} \int_{cell} e^{-i(\mathbf{G}-\mathbf{G}')\mathbf{r}} \Theta(\mathbf{r})d^3r \quad (70)$$

$$S_I^{\mathbf{G}\mathbf{G}'} = \frac{1}{\Omega} \int_{cell} e^{-i(\mathbf{G}-\mathbf{G}')\mathbf{r}} \Theta(\mathbf{r})d^3r \quad (71)$$

In momentum space Eq.(70) becomes:

$$H_I^{\mathbf{G}\mathbf{G}'}(\mathbf{k}) = (V\Theta)_{(\mathbf{G}-\mathbf{G}')} + \frac{\hbar^2}{2m}(\mathbf{G}' + \mathbf{k})^2\Theta_{(\mathbf{G}-\mathbf{G}')} \quad (72)$$

$$S_I^{\mathbf{G}\mathbf{G}'} = \Theta_{(\mathbf{G}-\mathbf{G}')} \quad (73)$$

Where $\Theta_{\mathbf{G}}$ and $(V\Theta)_{\mathbf{G}}$ are the Fourier coefficients of $\Theta(\mathbf{r})$ and $V(\mathbf{r})\Theta(\mathbf{r})$ respectively. Apparently these coefficients are needed up to a cut-off of $2G_{\max}$. The step function can be Fourier transformed analytically.

$$\Theta_{\mathbf{G}} = \delta_{\mathbf{G},\mathbf{0}} - \sum_{\mu} e^{-i\mathbf{G}\boldsymbol{\tau}^{\mu}} \frac{4\pi(R_{MT}^{\alpha})^3}{\Omega} \frac{j_1(GR_{MT}^{\alpha})}{GR_{MT}^{\alpha}}$$

where $\boldsymbol{\tau}^{\mu}$ indicates the position of atom μ . The Fourier transform of the product of $V(\mathbf{r})$ and $\Theta(\mathbf{r})$ is given by a convolution in momentum space.

$$(V\Theta)_{\mathbf{G}} = \sum_{\mathbf{G}'} V_{\mathbf{G}'}\Theta_{(\mathbf{G}-\mathbf{G}')}$$

This convolution depends on both, \mathbf{G} and \mathbf{G}' , therefore the numerical effort increases like $(G_{\max})^6$. However, $(V\Theta)_{\mathbf{G}}$ can be determined more efficiently, using Fast-Fourier-Transform (FFT). In Fig. 10 it is shown schematically how $(V\Theta)_{\mathbf{G}}$ can be obtained using FFT. Using this scheme the numerical effort increases like $(G_{\max})^3 \ln(G_{\max})^3$ with G_{\max} .

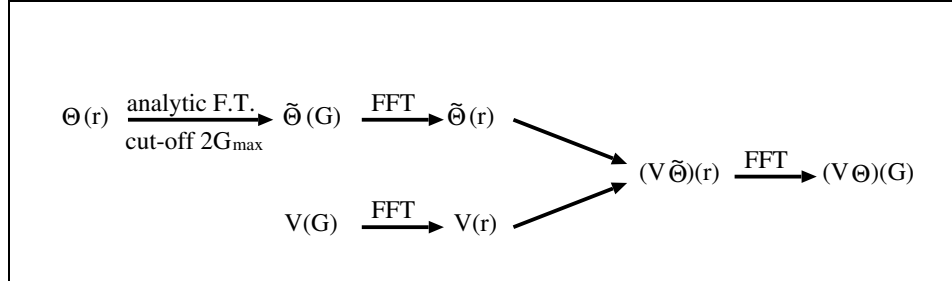


Figure 10. Schematic representation of the calculation of $(V\Theta)_{\mathbf{G}}$. First $\Theta(\mathbf{r})$ is Fourier transformed analytically with a cut-off of $2G_{\max}$ yielding $\tilde{\Theta}_{\mathbf{G}}$. Then $\tilde{\Theta}_{\mathbf{G}}$ and $V_{\mathbf{G}}$ are fast Fourier transformed and multiplied on a real space mesh. Finally, the result $(V\tilde{\Theta})(\mathbf{r})$ is back-transformed to momentum space.

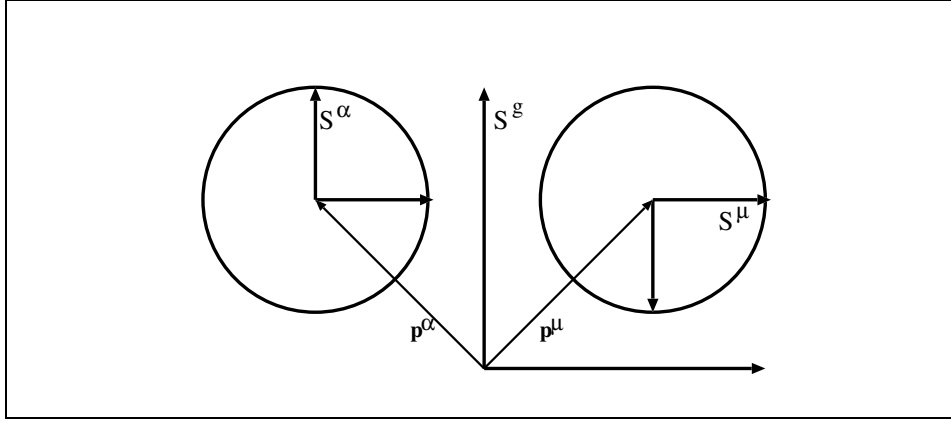


Figure 11. Local coordinate frames inside each muffin-tin.

4.2.3 The Muffin-Tin a- and b-Coefficients

Within FLAPW the electron wavefunctions are expanded differently in the interstitial region and the muffin-tins. Each basis function consists of a plane wave in the interstitial, which is matched to the radial functions and spherical harmonics in the muffin-tins. The coefficients of the function inside the spheres are determined from the requirement, that the basis functions and their derivatives are continuous at the sphere boundaries. These coefficients play an important role. In this section we will therefore discuss how the matching conditions can be solved and what properties they induce.

In many systems that the FLAPW method can be applied to some atoms are symmetry equivalent, i.e. these atoms can be mapped onto each other by a space group operation $\{R|\mathbf{t}\}$. Such a group of atoms is called an atom type, represented by one of the atoms. Let $\{R^\mu|\mathbf{t}^\mu\}$ the operation that maps the atom μ onto its representative. This atom can now be assigned a local coordinate frame S^μ (cf. Fig. 11), where the origin of S^μ is at the atoms position τ^μ . The local frame is chosen such that the unit vectors of the local frame S^μ are mapped onto those of the global frame by R^μ ($R^\mu S^\mu = S^g$). The local frame of the representative atom S^α is only translated with respect to the global frame, i.e. the same rotation R^μ maps S^μ onto S^α . The potential (and other quantities) inside the muffin-tins can now be written in terms of the local coordinate system. Due to the symmetry we find $V_{MT^\alpha}(\mathbf{r}^\alpha) = V_{MT^\mu}(\mathbf{r}^\mu)$, where \mathbf{r}^α and \mathbf{r}^μ are expanded in terms of the local frames S^α and S^μ respectively. As a consequence the radial functions $u_l(r)$ and the t-matrices are the same for all atoms of the same type. This way symmetry is exploited to save memory and computer time (during the calculation of the t-matrices).

Any plane wave can be expanded into spherical harmonics via the Rayleigh expansion.

$$e^{i\mathbf{K}\mathbf{r}} = 4\pi \sum_L i^l j_l(rK) Y_L^*(\hat{\mathbf{K}}) Y_L(\hat{\mathbf{r}}) \quad (74)$$

Where $r = |\mathbf{r}|$, $K = |\mathbf{K}|$ and \mathbf{K} abbreviates $(\mathbf{G} + \mathbf{k})$. Looked at from the local frame \mathbf{K} and τ^μ appear rotated, besides the origin of the local frame is shifted. Therefore, the

planewave has the following form in the local frame:

$$e^{i(\mathbf{R}^\mu \mathbf{K})(\mathbf{r} + \mathbf{R}^\mu \boldsymbol{\tau}^\mu)} \quad (75)$$

Thus, the Rayleigh expansion of the planewave in the local frame is given by:

$$e^{i\mathbf{K}\boldsymbol{\tau}^\mu} 4\pi \sum_L i^l j_l(rK) Y_L^*(\mathbf{R}^\mu \hat{\mathbf{K}}) Y_L(\hat{\mathbf{r}}) \quad (76)$$

The requirement of continuity of the wavefunctions at the sphere boundary leads to the equation:

$$\begin{aligned} & \sum_L a_L^{\mu\mathbf{G}}(\mathbf{k}) u_l(R_{MT^\alpha}) Y_L(\hat{\mathbf{r}}) + b_L^{\mu\mathbf{G}}(\mathbf{k}) \dot{u}_l(R_{MT^\alpha}) Y_L(\hat{\mathbf{r}}) \\ &= e^{i\mathbf{K}\boldsymbol{\tau}^\mu} 4\pi \sum_L i^l j_l(rK) Y_L^*(\mathbf{R}^\mu \hat{\mathbf{K}}) Y_L(\hat{\mathbf{r}}), \end{aligned} \quad (77)$$

where R_{MT^α} is the muffin-tin radius of the atom type α . The second requirement is, that the derivative with respect to r , denoted by $\partial/\partial r = \prime$, is also continuous.

$$\begin{aligned} & \sum_L a_L^{\mu\mathbf{G}}(\mathbf{k}) u_l'(R_{MT^\alpha}) Y_L(\hat{\mathbf{r}}) + b_L^{\mu\mathbf{G}}(\mathbf{k}) \dot{u}_l'(R_{MT^\alpha}) Y_L(\hat{\mathbf{r}}) \\ &= e^{i\mathbf{K}\boldsymbol{\tau}^\mu} 4\pi \sum_L i^l K j_l'(rK) Y_L^*(\mathbf{R}^\mu \hat{\mathbf{K}}) Y_L(\hat{\mathbf{r}}) \end{aligned} \quad (78)$$

These conditions can only be satisfied, if the coefficients of each spherical harmonic $Y_L(\hat{\mathbf{r}})$ are equal. Solving the resulting equations for $A_L^{\mu\mathbf{G}}(\mathbf{k})$ and $B_L^{\mu\mathbf{G}}(\mathbf{k})$ yields:

$$\begin{aligned} a_L^{\mu\mathbf{G}}(\mathbf{k}) &= e^{i\mathbf{K}\boldsymbol{\tau}^\mu} 4\pi \frac{1}{W} i^l Y_L^*(\mathbf{R}^\mu \hat{\mathbf{K}}) \\ & \quad [\dot{u}_l(R_{MT^\alpha}) K j_l'(R_{MT^\alpha} K) - \dot{u}_l'(R_{MT^\alpha}) j_l(R_{MT^\alpha} K)] \\ b_L^{\mu\mathbf{G}}(\mathbf{k}) &= e^{i\mathbf{K}\boldsymbol{\tau}^\mu} 4\pi \frac{1}{W} i^l Y_L^*(\mathbf{R}^\mu \hat{\mathbf{K}}) \\ & \quad [u_l'(R_{MT^\alpha}) j_l(R_{MT^\alpha} K) - u_l(R_{MT^\alpha}) K j_l'(R_{MT^\alpha} K)]. \end{aligned} \quad (79)$$

The Wronskian W is given by:

$$W = [\dot{u}_l(R_{MT^\alpha}) u_l'(R_{MT^\alpha}) - u_l(R_{MT^\alpha}) \dot{u}_l'(R_{MT^\alpha})] \quad (80)$$

4.3 Brillouin-Zone Integration and Fermi Energy

In the current implementation of the FLAPW method the Fermi energy is determined in two steps. First the bands are occupied (at all k-points simultaneously), starting from the lowest energy, until the sum of their weights equals the total number of electrons per unit cell, i.e. the discretized equivalent of Eq.(27) is solved at $T = 0$. Then, the step function is replaced by the Fermi and the Fermi energy is determined from the requirement that:

$$N = \sum_{\mathbf{k}} \sum_{\nu} w(\mathbf{k}, \epsilon_\nu(\mathbf{k}) - E_F) \quad (81)$$

Where the weights are given by:

$$w(\mathbf{k}, \epsilon_\nu(\mathbf{k}) - E_F) = w(\mathbf{k}) \frac{1}{e^{(\epsilon_\nu(\mathbf{k}) - E_F)/k_B T} + 1} \quad (82)$$

The weights $w(\mathbf{k}, \epsilon_\nu(\mathbf{k}) - E_F)$ are stored to be used for later Brillouin zone integrations.

4.4 Representation of the Density and the Potential

The expansion of the charge density n and the potential is very similar to expansion of the wavefunction. In the interstitial-region the two quantities are expanded into three-dimensional plane wave, inside the muffin-tins they are represented by spherical harmonics and radial functions, which are store on an exponential mesh and in the vacuum they are expanded into two-dimensional plane wave and z-depended functions, which are also given on an exponential mesh. However, the charge density is given by Eq.(1), which contains terms of the form $e^{i(\mathbf{G}-\mathbf{G}')\mathbf{r}}$. Consequently, for a consistent representation the charge density cut-off has to be twice the wavefunction cut-off G_{\max} . In Sect. 4.2.2 we explained, that the potential is also needed up to cut-off of $2G_{\max}$. This leads to a large number of coefficients, that need to be stored. Fortunately, this number can be reduced, if the symmetry of the system is exploited.

Of course, the charge density and the potential posses the lattice symmetry. Therefore, the expansion into plane waves is more general than necessary. The Plane waves can be replaced by symmetrized plane waves, the so called stars. They are defined by:

$$\Phi_s^{3D}(\mathbf{r}) = \frac{1}{N_{op}} \sum_{op} e^{i\mathbf{R}\mathbf{G}(\mathbf{r}-\mathbf{t})}, \quad (83)$$

where $\{\mathbf{R}|\mathbf{t}\}$ are the symmetry operation of the lattice space group; if all the translation vectors \mathbf{t} are zero, the space group is call symmorphic. By this construction all plane waves, that are symmetry equivalent, are combined to form one star. The two-dimensional stars $\Phi_s^{2D}(\mathbf{r})$ are defined in the same way, applying the operations of the two-dimensional space group only.

The same arguments can be applied to the expansion of the $n(V)$ inside the muffin-tins. In this case the relevant symmetry group is the point group of the atom under consideration. Thus, different expansions are used at different atoms in general. The symmetrized functions are called lattice harmonics and they are linear combinations of spherical harmonics

$$K_\nu(\hat{\mathbf{r}}) = \sum_m c_{\nu,m}^\alpha Y_L(\hat{\mathbf{r}}). \quad (84)$$

The lattice harmonics are real, orthonormal and invariant under the point group operations. Finally, the expansion of the the charge density has the form

$$n(\mathbf{r}) = \begin{cases} \sum_s n_s \Phi_s^{3D}(\mathbf{r}) & \mathbf{r} \in I \\ \sum_\nu n_\nu^\alpha(r) K_\nu(\hat{\mathbf{r}}) & \mathbf{r} \in MT^\alpha \end{cases} \quad (85)$$

The potential is expanded in exactly the same way.

4.5 Construction of the Electron Density

In this section we will discuss the determination of the charge density from the eigenfunctions. In density functional calculations of an infinite periodic solid, the electron density is given by an integral over the Brillouin zone (cf. Eq.(27)).

$$n(\mathbf{r}) = \frac{1}{V_{BZ}} \int_{BZ} \sum_{\nu, \epsilon_\nu(\mathbf{k}) < E_F} |\psi_\nu(\mathbf{k}, \mathbf{r})|^2 d^3k \quad (86)$$

Where V_{BZ} is the volume of the Brillouin zone, ν is the band index and E_F is the Fermi energy. In spin-polarized calculations the summation includes also the spin-index σ (cf. Sect.2.3), while in a non-magnetic calculation a factor “2” has to be added to account for the spin-degeneracy. In the case of film calculations the three-dimensional Brillouin zone is replaced by a two-dimensional Brillouin zone. In both cases integration methods that sample eigenfunctions and the eigenvalues on discrete k-point are used to compute the integrals. These methods transform the integration into a weighted sum over the k-points, where the choice of k-points and their weights depend on the integration method used. These weights depend not only on the k-point, but also on the energy of a band, i.e. on the band (index), because each band contributes to the electron density only if its energy is below the Fermi energy.

$$n(\mathbf{r}) = \sum_{\mathbf{k}} \sum_{\nu} |\psi_\nu(\mathbf{k}, \mathbf{r})|^2 w(\nu, \mathbf{k}) \quad (87)$$

Within the FLAPW method the eigenfunctions are represented in terms of the coefficients of the augmented planewaves.

$$\psi_\nu(\mathbf{k}, \mathbf{r}) = \sum_{\mathbf{G}} c_\nu^{\mathbf{G}}(\mathbf{k}) \varphi_{\mathbf{G}}(\mathbf{k}, \mathbf{r}) \quad (88)$$

Inside the muffin-tin spheres each planewave is coupled to a sum of spherical harmonics and radial functions. Hence, in a sphere μ an eigenfunction is given by:

$$\psi_\nu^\mu(\mathbf{k}, \mathbf{r}) = \sum_{\mathbf{G}} c_\nu^{\mathbf{G}}(\mathbf{k}) \sum_L a_L^{\mu\mathbf{G}}(\mathbf{k}) u_l^\alpha(r) Y_L(\hat{\mathbf{r}}) + b_L^{\mu\mathbf{G}}(\mathbf{k}) \dot{u}_l^\alpha(r) Y_L(\hat{\mathbf{r}}) \quad (89)$$

The $a_L^{\mu\mathbf{G}}(\mathbf{k})$ and $b_L^{\mu\mathbf{G}}(\mathbf{k})$ coefficients can be replaced by band dependent A- and B-coefficients, obtained by performing the contraction over the planewaves:

$$\psi_\nu^\mu(\mathbf{k}, \mathbf{r}) = \sum_L a_{L,\nu}^\mu(\mathbf{k}) u_l^\alpha(r) Y_L(\hat{\mathbf{r}}) + b_{L,\nu}^\mu(\mathbf{k}) \dot{u}_l^\alpha(r) Y_L(\hat{\mathbf{r}}), \quad (90)$$

where

$$A_{L,\nu}^\mu(\mathbf{k}) = \sum_{\mathbf{G}} c_\nu^{\mathbf{G}}(\mathbf{k}) a_L^{\mu\mathbf{G}}(\mathbf{k}), \quad B_{L,\nu}^\mu(\mathbf{k}) = \sum_{\mathbf{G}} c_\nu^{\mathbf{G}}(\mathbf{k}) b_L^{\mu\mathbf{G}}(\mathbf{k}). \quad (91)$$

4.5.1 “l-like” Charge

Since the wavefunctions are expanded into spherical harmonics inside the muffin-tin spheres, they can be split up into contributions with a certain l -character.

$$\psi_\nu^\mu(\mathbf{k}, \mathbf{r}) = \sum_l \psi_{\nu,l}^\mu(\mathbf{k}, \mathbf{r}) \quad (92)$$

The particle density of a certain state depends on the square of the wavefunction. Therefore, it contains cross-terms with a mixture of different l 's.

$$n_\nu^\mu(\mathbf{r}) = \frac{1}{V_{BZ}} \int_{BZ} \sum_l |\psi_{\nu,l}^\mu(\mathbf{k}, \mathbf{r})|^2 + \sum_{l'l} 2 \left(\psi_{\nu,l'}^\mu(\mathbf{k}, \mathbf{r}) \right)^* \psi_{\nu,l}^\mu(\mathbf{k}, \mathbf{r}) d^3k. \quad (93)$$

If, however, the density is integrated over the muffin-tin, the cross-terms vanish because of the orthogonality of the spherical harmonics. Thus, the total electron density inside a sphere can be written as a sum over contributions with definite l -character.

$$n_\nu^\mu = \sum_l n_{\nu,l}^\mu, \quad n_{\nu,l}^\mu = \frac{1}{V_{BZ}} \int_{BZ} \int_{MT^\mu} |\psi_{\nu,l}^\mu(\mathbf{k}, \mathbf{r})|^2 d^3r d^3k. \quad (94)$$

Where $n_{\nu,l}^\mu$ is called ‘‘ l -like’’ charge. We can also define a k -dependent l -like charge by:

$$n_{\nu,l}^\mu(\mathbf{k}) = \int_{MT^\mu} |\psi_{\nu,l}^\mu(\mathbf{k}, \mathbf{r})|^2 d^3r. \quad (95)$$

Substituting Eq.(90) yields:

$$n_{\nu,l}^\mu(\mathbf{k}) = \sum_{m=-l}^l |A_{L,\nu}^\mu(\mathbf{k})|^2 + |B_{L,\nu}^\mu(\mathbf{k})|^2 \dot{N}_l^\alpha, \quad (96)$$

where

$$\dot{N}_l^\alpha = \int_0^{R_{MT^\alpha}} (\dot{u}_l^\alpha(r))^2 r^2 dr \quad (97)$$

and the orthogonality of the spherical harmonics, the normalization of u_l^α and the orthogonality of u_l^α and \dot{u}_l^α have been used.

4.5.2 Determination of the Optimal Energy Parameter

In order to minimize the linearization error, the energy parameters should be chosen as close to the band energies as possible. However, the band energies $\epsilon_\nu(\mathbf{k})$ depend on \mathbf{k} whereas the energy parameters E_l^α are constants. In addition, the radial functions contribute to the eigenfunctions of different band with different energies. Therefore, deviations between $\epsilon_\nu(\mathbf{k})$ and E_l^α have to be accepted. An optimal choice can be obtained from the requirement, that the energy parameters minimize

$$\int_{BZ} \sum_{\nu, \epsilon_\nu(\mathbf{k}) < E_F} (\epsilon_\nu(\mathbf{k}) - E_l^\alpha)^2 n_{\nu,l}^\mu(\mathbf{k}) d^3k, \quad (98)$$

which is the quadratic error weighted with the amount of charge that each band contributes to the l -like charge with the l -character of the energy parameter. Setting the derivative $(\partial/\partial E_l^\alpha)$ equal to zero yields the optimal energy parameter:

$$E_l^\alpha = \left(\sum_{\mathbf{k}} \sum_{\nu} \epsilon_\nu(\mathbf{k}) n_{\nu,l}^\mu(\mathbf{k}) w(\nu, \mathbf{k}) \right) / \left(\sum_{\mathbf{k}} \sum_{\nu} n_{\nu,l}^\mu(\mathbf{k}) w(\nu, \mathbf{k}) \right) \quad (99)$$

4.5.3 Construction of the Electron Density in the Muffin-Tins

Substituting Eq.(90) into Eq.(86) yields the electron density in the muffin-tin spheres.

$$n^\mu(\mathbf{r}) = \frac{1}{V_{BZ}} \int_{BZ} \sum_{\nu, \epsilon_\nu(\mathbf{k}) < E_F} \sum_{L'} \left(A_{L',\nu}^\mu(\mathbf{k}) u_{l'}^\alpha(r) + B_{L',\nu}^\mu(\mathbf{k}) \dot{u}_{l'}^\alpha(r) \right)^* Y_{L'}^*(\hat{\mathbf{r}}) \sum_L \left(A_{L,\nu}^\mu(\mathbf{k}) u_l^\alpha(r) + B_{L,\nu}^\mu(\mathbf{k}) \dot{u}_l^\alpha(r) \right) Y_L(\hat{\mathbf{r}}) d^3k. \quad (100)$$

The particle density inside the muffin-tins is also expanded into spherical harmonics

$$n^\mu(\mathbf{r}) = \sum_L C_L^\mu(r) Y_L(\hat{\mathbf{r}}). \quad (101)$$

The coefficients $C_{L''}^\mu(r)$ can be determined by multiplying Eq.(100) with $\int d\Omega Y_{L''}(\hat{\mathbf{r}})$.

$$C_{L''}^\mu(r) = \frac{1}{V_{BZ}} \int_{BZ} \sum_{\nu, \epsilon_\nu(\mathbf{k}) < E_F} \sum_{L'} \left(A_{L',\nu}^\mu(\mathbf{k}) u_{l'}^\alpha(r) + B_{L',\nu}^\mu(\mathbf{k}) \dot{u}_{l'}^\alpha(r) \right)^* \sum_L \left(A_{L,\nu}^\mu(\mathbf{k}) u_l^\alpha(r) + B_{L,\nu}^\mu(\mathbf{k}) \dot{u}_l^\alpha(r) \right) G_{L''L}^{mm'm''} d^3k, \quad (102)$$

where it has been used, that the Gaunt coefficients are real, i.e.

$$\int Y_{lm} Y_{l'm'}^* Y_{l''m''}^* d\Omega = \int Y_{l'm'}^* Y_{lm} Y_{l''m''} d\Omega \quad (103)$$

Finally, applying a Brillouin zone integration method yields:

$$C_{L''}^\mu(r) = \sum_{l'l} \left(\sum_{\mathbf{k}} \sum_{\nu} \sum_{m'm} \left(A_{L',\nu}^\mu(\mathbf{k}) \right)^* A_{L,\nu}^\mu(\mathbf{k}) G_{L''L}^{mm'm''} w(\nu, \mathbf{k}) \right) u_{l'}^\alpha(r) u_l^\alpha(r) + \dots A^* B + B^* A + B^* B \dots \quad (104)$$

4.5.4 Construction of the Electron Density in the Interstitial Region

In the interstitial region the wavefunctions are represented in the following form.

$$\psi_\nu(\mathbf{k}, \mathbf{r}) = \sum_{\mathbf{G}} c_\nu^{\mathbf{G}}(\mathbf{k}) e^{i(\mathbf{G}+\mathbf{k})\mathbf{r}} \quad (105)$$

Starting from Eq.(1) the electron density is given by:

$$n(\mathbf{r}) = \frac{1}{V_{BZ}} \int_{BZ} \sum_{\nu, \epsilon_\nu(\mathbf{k}) < E_F} \sum_{\mathbf{G}'\mathbf{G}''} \left(c_\nu^{\mathbf{G}'}(\mathbf{k}) \right)^* c_\nu^{\mathbf{G}''}(\mathbf{k}) d^3k e^{i(\mathbf{G}''-\mathbf{G}')\mathbf{r}} \quad (106)$$

The electron density in the interstitial region is also expanded into planewaves.

$$n(\mathbf{r}) = \sum_{\mathbf{G}} n^{\mathbf{G}} e^{i\mathbf{G}\mathbf{r}} \quad (107)$$

Hence, the planewave coefficients of the electron density are:

$$n^{\mathbf{G}} = \frac{1}{V_{BZ}} \int_{BZ} \sum_{\nu, \epsilon_\nu(\mathbf{k}) < E_F} \sum_{\substack{\mathbf{G}'\mathbf{G}'' \\ \mathbf{G}''-\mathbf{G}'=\mathbf{G}}} \left(c_\nu^{\mathbf{G}'}(\mathbf{k}) \right)^* c_\nu^{\mathbf{G}''}(\mathbf{k}) d^3k \quad (108)$$

Apparently, the planewave cut-off of the particle density has to be twice the cut-off of the wavefunction expansion (G_{\max}) to allow an accurate description. The \mathbf{k} and state dependent density

$$n_{\nu}^{\mathbf{G}}(\mathbf{k}) = \sum_{\substack{\mathbf{G}'\mathbf{G}'' \\ \mathbf{G}''-\mathbf{G}'=\mathbf{G}}} \left(c_{\nu}^{\mathbf{G}'}(\mathbf{k})\right)^* c_{\nu}^{\mathbf{G}''}(\mathbf{k}) = \sum_{\mathbf{G}'} \left(c_{\nu}^{\mathbf{G}'}(\mathbf{k})\right)^* c_{\nu}^{(\mathbf{G}+\mathbf{G}')}(\mathbf{k}) \quad (109)$$

is given by a convolution in momentum space. For each coefficient a sum over \mathbf{G} has to be performed. Consequently, the numerical effort put into the determination of $n_{\nu}^{\mathbf{G}}(\mathbf{k})$ scales proportional to the number of G -vectors squared, i.e. proportional to $(G_{\max})^6$. However, $n_{\nu}^{\mathbf{G}}(\mathbf{k})$ can be calculated more efficiently using the fast Fourier transform (FFT). First, $c_{\nu}^{\mathbf{G}}(\mathbf{k})$ is Fourier transformed to real space, where it is squared on a real space mesh yielding $n_{\nu}(\mathbf{k}, \mathbf{r})$, then all states are summed up and finally the resulting particle density is back-transformed to momentum space.

$$c_{\nu}^{\mathbf{G}}(\mathbf{k}) \xrightarrow{FFT} \psi_{\nu}(\mathbf{k}, \mathbf{r}) \xrightarrow{square} n_{\nu}(\mathbf{k}, \mathbf{r}) \xrightarrow{\sum_{\nu}} n(\mathbf{k}, \mathbf{r}) \xrightarrow{FFT^{-1}} n^{\mathbf{G}}(\mathbf{k})$$

With this scheme the numerical effort increases proportional to $(G_{\max})^3 \ln G_{\max})^3$, which is a major improvement for large systems. In a last step the planewaves have to be combined to form the three-dimensional stars.

4.6 Construction of the Coulomb Potential

The Coulomb potential consists of two parts, the Hartree term $V_H(\mathbf{r})$ and the external potential of the nuclei $V_i(\mathbf{r})$.

$$V_c(\mathbf{r}) = V_H(\mathbf{r}) + V_i(\mathbf{r}) \quad (110)$$

The Hartree potential has to be determined from the charge density via the Poisson equation.

$$\Delta V_H(\mathbf{r}) = 4\pi n(\mathbf{r}) \quad (111)$$

In real space the solution of Eq.(111) is given by

$$V_H(\mathbf{r}) = \int \frac{4\pi n(\mathbf{r}')}{|\mathbf{r} - \mathbf{r}'|} d^3\mathbf{r}'. \quad (112)$$

In reciprocal space, however, the Poisson equation is diagonal, as a result the solution is very simple.

$$V_H(\mathbf{G}) = \frac{4\pi n(\mathbf{G})}{\mathbf{G}^2} \quad (113)$$

Therefore, and because of the representation of the charge density and the potential in the interstitial- and vacuum-region, the solution of the Poisson equation in reciprocal space appears to be convenient. However, due to the rather localized core and valence states the charge density changes on a very small length scale near the nuclei. Therefore, the planewave expansion of n convergences slowly, and a direct use of Eq.(113) is impractical, if not impossible. This difficulty can be circumvent via the pseudocharge method.

4.6.1 The Pseudocharge Method

The pseudocharge method, developed by Weinert²³, is a very elegant technique to calculate the interstitial and vacuum Hartree potential. The underlying idea is to divide the solution of the Poisson equation into two steps. In the first step the true muffin-tin charge is replaced by a convergent pseudocharge density \tilde{n} , that leads to the same potential outside the muffin-tins. Then, the interstitial (and vacuum) potential is calculated in reciprocal space. In the second step the muffin-tin potential is determined from the Dirichlet boundary value problem, defined by the exact muffin-tin charge and the interstitial potential on the muffin-tin sphere boundaries. The potential outside the the muffin-tin spheres due to a charge distribution inside the sphere is determined completely by its multipole moments q_L .

$$V(\mathbf{r}) = \sum_{l=0}^{\infty} \sum_{m=-l}^l \frac{4\pi}{2l+1} \frac{q_L}{r^{l+1}} Y_L(\hat{\mathbf{r}}), \quad (114)$$

However, the multipole moments do not define the charge density uniquely. The charge density is given by:

$$n(\mathbf{r}) = n_I(\mathbf{r})\Theta(\mathbf{r} \in I) + \sum_{\alpha} n_{\alpha}(\mathbf{r})\Theta(\mathbf{r} \in MT^{\alpha}) \quad (115)$$

Of course, in film calculation there is also a vacuum charge, and we will come back to this later. Eq.(115) can be rewritten

$$n(\mathbf{r}) = n_I(\mathbf{r}) + \sum_{\alpha} [n_{\alpha}(\mathbf{r}) - n_I(\mathbf{r})]\Theta(\mathbf{r} \in MT^{\alpha}). \quad (116)$$

Thus, the interstitial charge has been extended into the muffin-tin and subtracted there again. The second term in Eq.(116) can now be replaced by a pseudocharge \tilde{n}^{α} , that has the same multipole moments (cf.²³ for details). The resultant pseudocharge \tilde{n} is given by

$$\tilde{n}(\mathbf{r}) = n_I(\mathbf{r}) + \sum_{\alpha} \tilde{q}^{\alpha}(\mathbf{r}) \quad (117)$$

$\tilde{n}(\mathbf{r})$ is constructed to have a more rapidly converging Fourier expansion than the original charge density $n(\mathbf{r})$. Therefore, the Poisson equation can now be solved using Eq.(113).

Still, the muffin-tin potential V_{MT}^{α} remains to be determined. For this step the exact muffin-tin charge n_{α} has to be used. Since, the interstitial potential is already known at this point, the calculation of V_{MT}^{α} constitutes a classical spherically symmetric Dirichlet boundary value problem, which can be solved by the Green's function method⁷⁵.

$$V_{MT}^{\alpha}(\mathbf{r}) = \int_{MT^{\alpha}} n_{\alpha}(\mathbf{r}') G(\mathbf{r}, \mathbf{r}') d^3 r' - \frac{R_{\alpha}^2}{4\pi} \oint_{S^{\alpha}} V_I(\mathbf{r}') \frac{\partial G}{\partial n'} d\Omega' \quad (118)$$

The second integral is over the muffin-tin sphere boundary S^{α} , and it is necessary to satisfies the boundary conditions. The Green's function is given by:

$$G^{\alpha}(\mathbf{r}, \mathbf{r}') = 4\pi \sum_{l,m} \frac{Y_L(\hat{\mathbf{r}}') Y_L(\hat{\mathbf{r}})}{2l+1} \frac{r_{<}^l}{r_{>}^{l+1}} \left(1 - \left(\frac{r_{>}}{R_{MT^{\alpha}}} \right)^{2l+1} \right) \quad (119)$$

where $r_> = \max\{|\mathbf{r}|, |\mathbf{r}'|\}$, $r_< = \min\{|\mathbf{r}|, |\mathbf{r}'|\}$. Finally, the muffin-tin potential has to be expanded into lattice harmonics $K_\nu(\hat{\mathbf{r}})$.

$$V_{MT}^\alpha(\mathbf{r}) = \sum_\nu V_{MT,\nu}^\alpha(r) K_\nu(\hat{\mathbf{r}}) \quad (120)$$

The potential of the nuclei $V_i^\alpha(\mathbf{r}) = \frac{eZ_i^\alpha}{|\mathbf{r}|}$ is added to the spherical ($l = 0$) component of the potential $V_{MT,0}^\alpha(r)$.

The muffin-tin potential is computed in the same way for both, bulk and film calculations. Apparently, the interstitial and the vacuum have to be treated differently in the two cases, due to the different boundary conditions and the different representation of the vacuum potential. Therefore, the next two sections the solution of the Poisson equation will be outlined separately for these cases in.

4.6.2 Determination of the Interstitial Coulomb Potential in Bulk Calculations

In the case of bulk calculations we have periodic boundary conditions in three dimensions. Therefore, the solution of the Poisson equation,

$$\mathbf{G}^2 V(\mathbf{G}) = 4\pi\tilde{n}(\mathbf{G}) \quad (121)$$

is very simple. Obviously, this equation can only be solved, if $\tilde{n}(0) = 0$. Since $\tilde{n}(0)$ is the average charge density, this means, that charge neutrality is essential. Still, $V(0)$ remains undetermined by Eq.(121), i.e. one has the freedom to shift the potential by a constant. This is a consequence of the periodic boundary conditions, because they do not fix the reference of the potential. Usually $V(0)$ is chosen to be zero, hence the Coulomb potential in the interstitial-region is given by:

$$V_I(\mathbf{r}) = \sum_{\mathbf{G} \neq 0} \frac{4\pi\tilde{n}(\mathbf{G})}{\mathbf{G}^2} e^{i\mathbf{G}\mathbf{r}} = \sum_{s \neq 0} \frac{4\pi\tilde{n}_s}{\mathbf{G}_s^2} \Phi_s^{3D}(\mathbf{r}) \quad (122)$$

where the first summation is expressed in terms of G -vectors and the second in terms of stars.

4.7 Computation of the Exchange Correlation Potential

The problem of the determination of the exchange correlation potential is quite different from the Coulomb potential. On one hand, V_{xc}^σ is a local quantity, i.e. $V_{xc}^\sigma(\mathbf{r})$ depends only on $n_\uparrow(\mathbf{r})$ and $n_\downarrow(\mathbf{r})$ at the same position \mathbf{r} . Thus, the muffin-tins, the interstitial- and vacuum-region can be treated independently. On the other hand, V_{xc}^σ and ϵ_{xc}^σ are non-linear functions of n_\uparrow and n_\downarrow . Therefore, V_{xc}^σ and ϵ_{xc}^σ have to be calculated in real space. V_{xc}^σ and ϵ_{xc}^σ are determined in the same way. First, n_\uparrow and n_\downarrow are transformed to real space, where V_{xc}^σ and ϵ_{xc}^σ are calculated. Then, V_{xc}^σ and ϵ_{xc}^σ are back-transformed. Then, V_{xc}^σ is added to the Coulomb potential, yielding the spin-dependent potential V_\uparrow and V_\downarrow . ϵ_{xc}^σ is needed for the determination of the total energy.

4.7.1 Calculation of ϵ_{xc}^σ and V_{xc}^σ in the Interstitial-Region

In the interstitial-region the charge density is expanded into three-dimensional stars with coefficients n_s^σ . Multiplying these by $e^{i\mathbf{R}\mathbf{G}t}$ yields the planewave coefficients n_G^σ . If the space group is symmorphic the star and planewave coefficients are identical. However, due to numerical inaccuracy, the calculated coefficients of symmetry equivalent planewaves are not exactly equal, and the corresponding star coefficient is obtained from the average of the planewave coefficients. In the next step a three-dimensional Fast-Fourier transform is carried out. Then, the exchange correlation potential is calculated on a real space mesh \mathbf{r}_i . Finally, V_{xc}^σ is back-transformed, and the star coefficients are computed.

$$n_s^\sigma \longrightarrow n_G^\sigma \xrightarrow{FFT} n^\sigma(\mathbf{r}_i) \longrightarrow V_{xc}^\sigma(\mathbf{r}_i) \xrightarrow{FFT^{-1}} V_{xc}^{\sigma,G} \longrightarrow V_{xc}^{\sigma,s}.$$

4.7.2 Calculation of ϵ_{xc}^σ and V_{xc}^σ in the Muffin-Tin Spheres

The muffin-tin charge is expanded into lattice harmonics and radial functions. The radial functions are stored on a discrete real-space mesh. Thus, the transform to real space affects only the angular part. The charge density is calculated on a set of special angular points $\hat{\mathbf{r}}_i = (\theta_i, \phi_i)$. Again, the exchange correlation potential is calculated in real space. Thereafter, the result $V_{xc}^\sigma(\mathbf{r})$ is expanded into spherical harmonics Y_L . The Y_L are orthonormal, therefore the coefficients can be obtained from

$$v_{xc,L}^\sigma(r) = \int Y_L(\hat{\mathbf{r}}) V_{xc}^\sigma(r, \hat{\mathbf{r}}) d\Omega. \quad (123)$$

The choice of the points $\hat{\mathbf{r}}_i = (\theta_i, \phi_i)$, on which $n^\sigma(\mathbf{r})$ and $V_{xc}^\sigma(\mathbf{r})$ are calculated, depends on the integration method, that is used to perform the angular integration. In the current implementation Eq.(123) is computed via a Gauß-Legendre integration and the angular points are chosen such, that the orthonormality condition of the Y_L holds also for the angular mesh $\hat{\mathbf{r}}_i$.

5 The FLAPW-Method for Specialized Geometries

5.1 The Film Geometry for Surfaces and Thin Films

Today, the physics of surfaces and films is an field of major interest and investigation. However, surfaces are difficult to treat, because they break the translational symmetry, i.e. there is only the 2-dimensional symmetry parallel to the surface left to be used to reduce the problem, and a semi-infinite problem is left perpendicular to the surface. In our approach surfaces are approximated by thin films, typically 10–15 atomic layers thick. Obviously, this approximation, which is called the thin-slab approximation, can only yield good results if the interaction between the two surfaces of the film is week enough, so that each of them shows the properties of the surfaces of an ideal semi-infinite crystal. In the case of film calculations space is divided into three distinct regions, the muffin-tins, the interstitial and the vacuum region (cf. Fig. 12). The interstitial region now stretches from $-D/2$ to $D/2$ in z-direction, which is defined to be the direction perpendicular to the film. The representation of the wavefunctions inside the muffin-tin spheres remains exactly the same as in the bulk case. Since the periodicity along the z-direction is lost, the unit cell

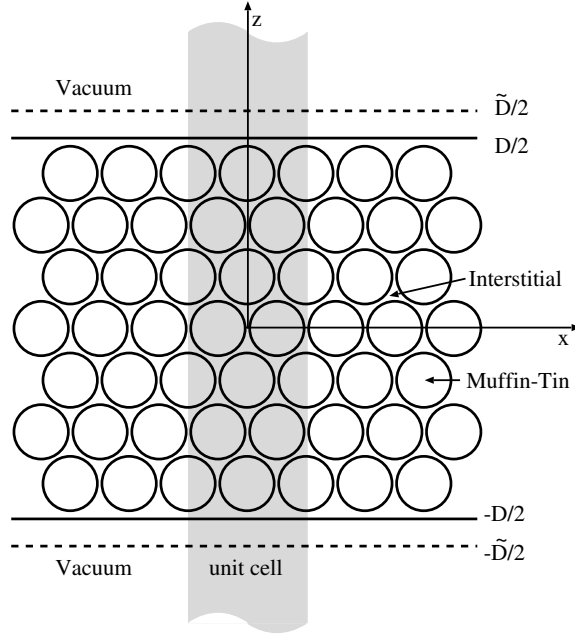


Figure 12. The unit cell in film calculations contain two semi-infinite vacuum regions.

extends principally from $-\infty$ to ∞ in z -direction. Still the wavefunctions can be expanded in terms of planewaves. However, the wavevectors perpendicular to the film are not defined in terms of D , but in terms of \tilde{D} , which is chosen larger than D to gain greater variational freedom. Therefore, the planewaves have the form

$$\varphi_{\mathbf{G}_{\parallel}G_{\perp}}(\mathbf{k}_{\parallel}, \mathbf{r}) = e^{i(\mathbf{G}_{\parallel} + \mathbf{k}_{\parallel})\mathbf{r}_{\parallel}} e^{iG_{\perp}z} \quad \text{with} \quad G_{\perp} = \frac{2\pi n}{\tilde{D}}, \quad (124)$$

where \mathbf{G}_{\parallel} and \mathbf{k}_{\parallel} are the 2-dimensional wave- and Bloch vectors, \mathbf{r}_{\parallel} is the parallel component of \mathbf{r} and G_{\perp} is the wavevector perpendicular to the film. The basis functions in the vacuum region are constructed in the same spirit as the functions in the muffin-tins. They consist of planewaves parallel to the film, and a z -dependent function $u_{\mathbf{G}_{\parallel}}(\mathbf{k}_{\parallel}, z)$, which solves the corresponding one-dimensional Schrödinger equation Eq.(125), plus its energy derivative $\dot{u}_{\mathbf{G}_{\parallel}}(\mathbf{k}_{\parallel}, z)$.

$$\left\{ -\frac{\hbar^2}{2m} \frac{\partial^2}{\partial z^2} + V_0(z) - E_{vac} + \frac{\hbar^2}{2m} (\mathbf{G}_{\parallel} + \mathbf{k}_{\parallel})^2 \right\} u_{\mathbf{G}_{\parallel}}(\mathbf{k}_{\parallel}, z) = 0 \quad (125)$$

E_{vac} is the vacuum energy parameter and $V_0(z)$ is the planar averaged part of the vacuum potential. As in the case of \dot{u}_i in the muffin-tins, the function $\dot{u}_{\mathbf{G}_{\parallel}}(\mathbf{k}_{\parallel}, z)$ is calculated from a Schrödinger-like equation, which can be obtained by deriving Eq.(125) with respect to the energy.

$$\left\{ -\frac{\hbar^2}{2m} \frac{\partial^2}{\partial z^2} + V_0(z) - E_{vac} + \frac{\hbar^2}{2m} (\mathbf{G}_{\parallel} + \mathbf{k}_{\parallel})^2 \right\} \dot{u}_{\mathbf{G}_{\parallel}}(\mathbf{k}_{\parallel}, z) = u_{\mathbf{G}_{\parallel}}(\mathbf{k}_{\parallel}, z) \quad (126)$$

The resulting basis functions have the form

$$\varphi_{\mathbf{G}_{\parallel}G_{\perp}}(\mathbf{k}_{\parallel}, \mathbf{r}) = \{a_{\mathbf{G}_{\parallel}G_{\perp}}(\mathbf{k}_{\parallel})u_{\mathbf{G}_{\parallel}}(\mathbf{k}_{\parallel}, z) + b_{\mathbf{G}_{\parallel}G_{\perp}}(\mathbf{k}_{\parallel})\dot{u}_{\mathbf{G}_{\parallel}}(\mathbf{k}_{\parallel}, z)\} e^{i(\mathbf{G}_{\parallel}+\mathbf{k}_{\parallel})\mathbf{r}_{\parallel}} \quad (127)$$

The coefficients $a_{\mathbf{G}_{\parallel}G_{\perp}}(\mathbf{k}_{\parallel})$ and $b_{\mathbf{G}_{\parallel}G_{\perp}}(\mathbf{k}_{\parallel})$ are determined in exactly the same way as it is done for the muffin-tins by requiring that the functions are continuous and differentiable at the vacuum boundary. It should be mentioned, that the vacuum basis functions offer less variational freedom than the basis set in the interstitial region does. This can be seen by noting that there are only two functions, $u_{\mathbf{G}_{\parallel}}$ and $\dot{u}_{\mathbf{G}_{\parallel}}$ times the corresponding planar plane-wave, to be matched to all plane-waves of the interstitial region with the same \mathbf{G}_{\parallel} . But there are generally far more than two different G_{\perp} 's, i.e the number of basis functions in the vacuum region is significantly smaller than in the interstitial region. However, this can be improved rather easily. In Eq.(125) only one energy parameter E_{vac} is used. Instead one can use a whole series of parameters E_{vac}^i to cover an energy region. A possible choice of the energy parameters could be $E_{vac}^i = E_{vac}^{G_{\perp}} = E_{vac} - \frac{\hbar^2}{2m}G_{\perp}^2$, which leads correspondingly to G_{\perp} dependent basis functions $u_{\mathbf{G}_{\parallel}G_{\perp}}(\mathbf{k}_{\parallel}, z)$. For more details see Ref.⁷⁶. In general, however, the present approximations is accurate, the energy spectrum of the electrons in the vacuum region is small due to the work-function.

Finally we would like to summarize the basis set used for thin film calculation with the FLAPW method.

$$\varphi_{\mathbf{G}_{\parallel}G_{\perp}}(\mathbf{k}_{\parallel}, \mathbf{r}) = \begin{cases} e^{i(\mathbf{G}_{\parallel}+\mathbf{k}_{\parallel})\mathbf{r}_{\parallel}} e^{iG_{\perp}z} & \text{interstitial} \\ \{a_{\mathbf{G}_{\parallel}G_{\perp}}(\mathbf{k}_{\parallel})u_{\mathbf{G}_{\parallel}}(\mathbf{k}_{\parallel}, z) \\ + b_{\mathbf{G}_{\parallel}G_{\perp}}(\mathbf{k}_{\parallel})\dot{u}_{\mathbf{G}_{\parallel}}(\mathbf{k}_{\parallel}, z)\} e^{i(\mathbf{G}_{\parallel}+\mathbf{k}_{\parallel})\mathbf{r}_{\parallel}} & \text{vacuum} \\ \sum_L a_L^{\mu\mathbf{G}}(\mathbf{k})u_l(r)Y_L(\hat{\mathbf{r}}) + b_L^{\mu\mathbf{G}}(\mathbf{k})\dot{u}_l(r)Y_L(\hat{\mathbf{r}}) & \text{MT}^{\mu} \end{cases} \quad (128)$$

This expansion has been suggested by H. Krakauer, M. Posternak and A. J. Freeman³¹. Correspondingly, the charge density and potential is expanded in the form:

$$n(\mathbf{r}) = \begin{cases} \sum_s n_s \Phi_s^{3D}(\mathbf{r}) & \mathbf{r} \in \text{interstitial region} \\ \sum_s n_s(z) \Phi_s^{2D}(\mathbf{r}) & \mathbf{r} \in \text{vacuum} \\ \sum_{\nu} n_{\nu}^{\mu}(r) K_{\nu}(\hat{\mathbf{r}}) & \mathbf{r} \in \text{MT}^{\mu} \end{cases} \quad (129)$$

and the Hamiltonian and overlap matrix consists now of an additional term (compare to Eq.(55)), the vacuum contribution, paying tribute that the space is now partitioned in three regions

$$H = H_I + H_{MT} + H_V \quad \text{and} \quad S = S_I + S_{MT} + S_V. \quad (130)$$

$n_s(z)\Phi_s^{2D}$ contains important information for the analysis and interpretation of STM topography and spectroscopy results on the basis of the Tersoff-Hamann model⁷⁷ as worked out by Heinze *et al.*⁷⁸.

5.2 The Wire Geometry for Chains, Wires and Tubes

In the FLAPW method for one-dimensional systems⁴⁶, the infinite three-dimensional space is again partitioned into three regions: the muffin-tin spheres around the atoms, the interstitial region between the atoms and within a cylinder along the axis of the wire (z) of the

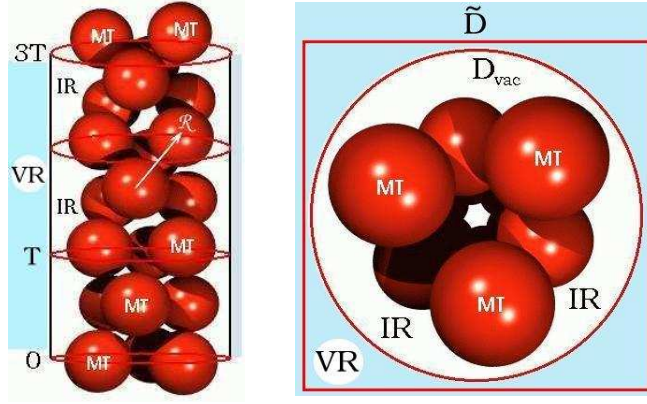


Figure 13. Spatial partitioning of space into muffin-tin spheres (MT), interstitial region (IR) and vacuum region (VR) (shown in blue color) is shown from aside (left) and from the top (right). The vacuum region is the infinite region outside the cylinder with the diameter D_{vac} . In-plane reciprocal vectors \mathbf{G}_{\parallel} are generated in an in-plane square lattice with the lattice constant $\tilde{D} > D_{\text{vac}}$.

radius R_{vac} . Outside this cylinder there is an infinitely extended vacuum region (VR in Fig. 13). From here on we define the z -axis as the axis of one-dimensional translational symmetry. As our method is based on the use of LAPW basis functions,^{19,31,12} the set of reciprocal vectors $\mathbf{G} = (\mathbf{G}_{\parallel}, G_z)$ is generated in a rectangular box, which reflects the translational periodicity of the system in z -direction. The corresponding Bloch number, k_z , lies within the first one-dimensional Brillouin zone. The in-plane reciprocal lattice vectors \mathbf{G}_{\parallel} are generated in an in-plane square lattice with the lattice constant \tilde{D} . The vacuum region is an infinite region outside the cylinder with the diameter $D_{\text{vac}} < \tilde{D}$ ($D_{\text{vac}} = 2R_{\text{vac}}$), with the axis along z -direction.

As characteristic for the FLAPW method, optimally adjusted basis functions are used in three different regions of space. In the interstitial region and in the spheres, the usual LAPW basis functions are used. In the vacuum the following representation is used:

$$\varphi_{\mathbf{G}}(k_z, \mathbf{r}) = \sum_m \left(a_m^{\mathbf{G}}(k_z) u_m^{G_z}(k_z, r) + b_m^{\mathbf{G}}(k_z) \dot{u}_m^{G_z}(k_z, r) \right) e^{im\varphi} e^{i(G_z + k_z)z}. \quad (131)$$

The space coordinate \mathbf{r} is written in terms of cylindrical coordinates (r, φ, z) and the summation over m goes up to the angular expansion parameter m_{max} , which ensures that the oscillations of the plane-waves on the cylindrical vacuum boundary continue smoothly to the vacuum side. Since the vacuum potential is rather flat, relativistic effects on the basis functions can safely be ignored, and the cylindrically symmetrical part of the vacuum potential $V_0(r)$ and the vacuum energy parameter E_v , determined in every iteration, enter in solving the radial Schrödinger equation for every pair (m, G_z) giving rise to the vacuum radial basis wavefunctions $u_m^{G_z}(k_z, r)$ and their energy derivatives $\dot{u}_m^{G_z}(k_z, r)$.

The sets of augmentation coefficients a and b both for the MT spheres and the vacuum region are determined such that the basis functions and their spatial derivatives are continuous across the MT spheres, interstitial and vacuum region boundaries. All the basis functions with reciprocal lattice vector \mathbf{G} that fulfill the condition $|k_z + \mathbf{G}| < K_{\text{max}}$ are

included. The corresponding representation of the charge density and potential involves all vectors \mathbf{G} with $|\mathbf{G}| < G_{\max}$. Typically, $G_{\max} \approx 3 \cdot K_{\max}$ in order to describe multiplication of the interstitial potential with the step function. The vacuum parameter m_{\max} is defined in the same manner as l_{\max} in the spheres:¹⁴ $m_{\max} \simeq K_{\max} \cdot R_{\text{vac}}$.

6 Where has the CPU Time gone

A thorough understanding where and how much CPU time is spent during a FLAPW calculation is compulsory to judge which problems can be solved with given computers and to develop strategies to overcome possible limitations. Along the discussion of two possible paths to speed-up the calculations put forward in the following two sections, we estimate of CPU time requests for different parts of the FLAPW-method as implemented in the FLEUR code³⁰.

6.1 Using Symmetry to speed-up Calculations

As surface science is an important field of materials science and condensed matter physics, in this section we compare the very efficient film approach (see Sect. 5.1) to simulate surfaces in electronic structure calculations with the very popularly used repeated slab model within a super-cell approach, where the unit cell consists of a film of a finite number of layers of a material and empty space describing the vacuum and the decoupling of the films from unit cell to unit cell. To repeat what has been said in Sect. 5.1, the key fact is, that the film approach reduces the number of LAPW basis functions N_{APW} as compared to the super-cell model.

To illustrate the effect, we choose as reference system a calculation of a 9-layer film of Cu(110) with a single \mathbf{k} -point in a $p(4 \times 2)$ unit cell containing 72 atoms. This system was also chosen in performance tests of the unparallelized WIEN-code^{79,80}) offers to possibility to gauge different implementations of the same method. Our calculations were performed with equivalent cutoff parameters also on a single node IBM/RS 6000 AIX-SP2 system to facilitate a comparison of the run times. We made no attempt to optimize the code for a certain architecture. In comparison to a repeated slab calculation ($N_{\text{APW}} = 7069$), the film geometry ($\tilde{D} = 30$ a.u.) reduces N_{APW} by approx. 1000 or 14%. This reduces the computational effort in the Hamiltonian setup (scaling with N_{APW}^2) by 27%, in the diagonalization ($\propto N_{\text{APW}}^3$) by 37% (cf. chart in Fig.14). Potential generation (linear with N_{APW}) and charge density construction for the IR (this is done via discrete FFT and scales with $N_{\text{APW}} \ln(N_{\text{APW}})$) are moderately affected.

Our reference system, as well as many other systems of interest, possesses inversion symmetry. In the above calculation, we exploited this fact already, solving a symmetric rather than an hermitian eigenvalue problem, saving time and memory. But a further benefit can be drawn from this symmetry: The augmentation coefficients $P_{L,\mu}^{\mathbf{k},\mathbf{G}}$ ($P = a, b$ cf. Eq.(79)) for an atom μ at a position τ_μ are evaluated as

$$P_{L,\mu}^{\mathbf{k},\mathbf{G}} = 4\pi i^l e^{i(\mathbf{k}+\mathbf{G}) \cdot \tau_\mu} f_l(x) Y_L^*(\widehat{\mathbf{k}+\mathbf{G}}) \quad (132)$$

where R_μ is the MT radius and $f_l(x)$ is a linear combination of Bessel functions of argument $x = (k + G)R_\mu$. This time consuming evaluation has to be done for all atoms in the

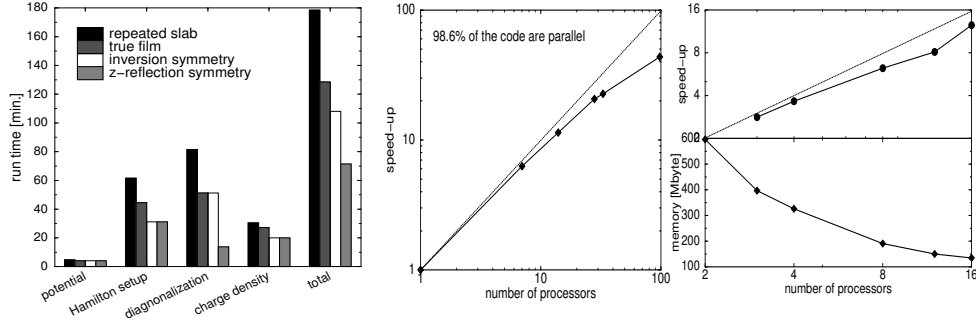


Figure 14. Left: Breakup of the computing time for a calculation of the p(4 × 2) Cu(110) film. The run-times are given for a repeated slab model, a true film calculation, and the latter with making use of inversion and z-reflection symmetry. The total time of 178 min. per self-consistency cycle should be compared to 174 min. obtained with the optimized WIEN code⁸⁰ at the same computer using standard diagonalization and otherwise similar cutoff parameters. Middle: Speed-up from the parallelization over the \vec{k} -points for a 9-layer film of Fe(100) with 196 k-points. Right: Speed-up and memory requirements due to eigenvector parallelization tested on a 9-layer film of p(4 × 2) Cu(110) with a single k-point on a Cray T3E. The memory requirements for the calculation with two processors was extrapolated and a similar value was also found for the unparallelized calculation.

Hamiltonian as well as in the charge density setup. If two equivalent atoms μ and μ' are connected by inversion symmetry, then $-\tau_\mu = \tau_{\mu'}$ and therefore it is easily verified from Eq.(132) that $P_{L,\mu'}^{\mathbf{k},\mathbf{G}} = (-1)^{l+m} (P_{L,-m,\mu}^{\mathbf{k},\mathbf{G}})^*$. This simple relation helps to speed-up both the matrix setups and the charge density generation. In our specific example 44% of the coefficients can be constructed in this way. The actual speed-up gained from this procedure can be seen in the chart of Fig. 14.

A film with a mirror plane perpendicular to its surface normal (which shall point in z-direction), i.e. z-reflection symmetry, allows the use of symmetrized basis functions³¹:

$$\chi_{\mathbf{k}_\parallel, \mathbf{G}}^\pm(\mathbf{r}) = \sqrt{2} e^{i(\mathbf{k}_\parallel + \mathbf{G}_\parallel) \cdot \mathbf{r}_\parallel} \begin{cases} \cos(G_z z); (+) \\ \sin(G_z z); (-) \end{cases} \quad (133)$$

where $\mathbf{G} = (\mathbf{G}_\parallel, G_z)$. Here we exploit the fact, that in film-calculations $\mathbf{k} = \mathbf{k}_\parallel$. Therefore, not only the density and potential, but also the basis functions have z-reflection symmetry. This enables a block-diagonalization of the eigenvalue problem, decomposing the Hamilton- and overlap matrix into symmetric and antisymmetric blocks. Apart from a small overhead – resulting from sorting the eigenvectors – we expect a speed-up of a factor 4 for a N_{APW}^3 scaling diagonalization routine. From the chart in Fig. 14 one finds that this value is almost obtained. In summary, we gained a speed-up of more than a factor 2.5 as compared to a repeated slab calculation where these symmetries were neglected.

Using the same concept for one-dimensional systems, compared to the conventional FLAPW formulation, the 1D-method can be 150 times faster than the supercell approach, and the Hamiltonian construction and the diagonalization part of the 1D code even 270 times faster than that of the bulk super-cell code⁴⁶. As compared to the supercell approach using the film geometry, per self-consistency iteration the 1D-method is then 15 times faster, and the Hamiltonian construction and the diagonalization part of the 1D code is 25 times faster than that of the film super-cell code.

6.2 Parallelization of the Algorithm

Due to the rather complex algorithm of a FLAPW-program as compared to a quantum Monte Carlo code for instance, there is no straight forward parallelization strategy. From the chart in Fig. 14 it is evident that there is no single, well-defined part of the program that consumes almost all computer-time. Moreover, depending on the actual problem, the computational costs are distributed quite differently: while in large systems most of the time is spent in the diagonalization of the eigenvalue problem, in systems of moderate size other parts of the code might get equally time consuming. But even small systems can become supercomputer applications when the eigenvalue problem has to be solved for a huge number of k -points, N_k , as it is required in many magnetic problems. Applications on workstation clusters require a minimization of communication between the nodes, while on massively parallel machines the memory requirements for the setup of the Hamilton matrix may surpass the resources available on a single processor. This calls for flexible parallelization strategies.

To fulfill adequately the needs of all different kinds of calculations we introduced parallelization on two levels: a coarse grained k -point parallelization and a fine grained combined eigenvector and eigenvalue parallelization. Depending on the actual values of N_k and the number of processors, N_{pe} , available for the application as well as on the memory-resources on the individual processors, the simultaneous application of both strategies allows a flexible load balancing.

k point parallelization: For a calculation of the $p(4 \times 2)$ Cu(110) surface with only one k -point we find that 92.6% of the time was spent in the k -dependent part of the code, whereas the rest was used mainly for the potential construction (5.7%). From this we expect that the k -point parallelization will be a very efficient strategy beyond one k -point.

In the parallelized version of the FLEUR-code the setup and the potential construction are done on a single processor. All necessary variables are then broadcasted to the other processors and the potential can be read from a file if there is a common file system for all nodes. The eigenvalue problem that has to be solved for all k -points can now be distributed over the processors and the results (eigenvalues and -vectors) are written to a global direct-access file. If no common filesystem exists, each node may write the results to a private file and send the eigenvalues back to the node that did the setup and which determines now the Fermi-level. With this result, the occupancy of the eigenvalues can be calculated and the result is sent to all processors. With this information all nodes can calculate a partial charge density (and e.g. forces on the atoms, orbital moments etc.) from the eigenvectors that were calculated in the last step. Up to this point the communication between the nodes was almost negligible, but now the charge densities from all nodes are sent back to and summed up by the first node. Here, the charge density mixing and all necessary output is done that finishes a step of the self-consistency cycle.

Since there is no additional computational effort and a moderate amount of communication between the nodes, the performance is almost ideal. In case of the film containing 72 Cu atoms a parallelization of more than 92% can be expected from the unparallelized calculation. But the performance is also splendid for smaller systems as it is shown in Fig. 14. Test was carried out for a 196 k -point calculation as it occurs typically in the connection with calculations of the magnetic anisotropy calculations where often even a denser sampling of the Brillouin zone is necessary.

Eigenstate parallelization: Due to memory (per node) limitations on massively parallel

machines, \mathbf{k} -point parallelization alone does not suffice to calculate big systems. In this case one distributes the eigenvalue problem for each \mathbf{k} -point on $N_{\text{pe}}^{\text{ev}}$ nodes.

We found it most useful to adopt a parallel QR-algorithm for the solution of the generalized (symmetric or hermitian) eigenvalue problem that uses the matrices in a column-wise distributed fashion, i.e. a column i of the Hamilton and overlap matrix can be found on the processor with the number $\text{mod}(i, N_{\text{pe}}^{\text{ev}})$. Since our matrices are symmetric or hermitian we calculate only one part of every column, the other part is sent from the other nodes to complete the column. Compared to the unparallelized code, where packed matrices are used, this gives us no big improvement on the use of memory if $N_{\text{pe}}^{\text{ev}} = 2$, but when four processors work on one \mathbf{k} -point we use only half of the memory per node for the matrices (and they normally use most of the memory in this step). Since the communication is moderate and no additional computational effort arises for the matrix setup, the scaling of this part with the number of processors is almost linear. The parallel QR-algorithm reduces the generalized eigenvalue problem via a Cholesky-factorization (see also Sect. 2.4) to a normal one and uses a Householder transform to get a tridiagonal matrix. From this matrix the ($\approx 10\%$) lowest eigenvalues are determined and the eigenvector calculation is distributed over the $N_{\text{pe}}^{\text{ev}}$ nodes. Finally, each processor holds approximately the same number of eigenvalue/eigenvector pairs.

For the determination of the charge density there is no conceptual difference whether each node calculates a partial charge density from a subset of \mathbf{k} -points or from a subset of eigenvalues of a selected \mathbf{k} -point. Therefore, it is rather easy to implement a parallelized charge-density generator once the complete eigenvectors are available on the nodes. The efficiency of this parallelization strategy for the Cu(110) reference system is shown in the right panel of Fig. 14.

The parallelization of FLAPW-codes enabled calculations of systems with unprecedented complexity involving unit cells of several hundredth of atoms dealing simultaneously with complex magnetic structures. The strategy of parallelization presented combines the flexibility required to tackle very different problems with transparency in the source-code and an acceptable performance on various parallel computer platforms.

Acknowledgments

This article benefited from discussions and collaborations with Henry Krakauer, Eugene Krasovskii, Philipp Kurz, Yuri Mokrousov, Rositza Pentcheva, Josef Redinger and Mike Weinert, which took place over a long period of time.

References

1. H. Hohenberg and W. Kohn, *Inhomogeneous Electron Gas*, Phys. Rev. **136**, B864 (1964).
2. R. M. Dreizler and J. da Provincia, *Density Functional Methods in Physics* (Plenum, New York, 1985).
3. R. O. Jones and O. Gunnarsson, *The density functional formalism, its applications and prospects*, Rev. Mod. Phys. **61**, 689 (1989).

4. M. Ernzerhof, J. P. Perdew and K. Burke, *Density Functionals: Where do they come from, why do they work?*, in *Topics in Current Chemistry*, Vol. 180, R.F. Nalewajski Ed. (Springer, Berlin, 1996).
5. A. Zunger and A. J. Freeman, *Ground-state electronic properties of diamond in the local-density formalism*, Phys. Rev. B **15**, 5049 (1977).
6. V. L. Moruzzi, J. F. Janak and A. R. Williams, *Calculated Electronic Properties of Metals* (Pergamon, New York, 1978).
7. E. Runge and E. K. U. Gross, *Density-Functional Theory for Time-Dependent System*, Phys. Rev. Lett. **52**, 997 (1984).
8. M. Petersilka, U. J. Gossmann, and E. K. U. Gross, *Excitation Energies from Time-Dependent Density-Functional Theory*, Phys. Rev. Lett. **76**, 1212 (1996).
9. J. D. Talman and W. F. Shadwick, *Optimized effective atomic central potential*, Phys. Rev. A **14**, 36 (1976)
10. V. I. Anisimov, A. I. Poteryaev, M. A. Korotin, A. O. Anokhin, and G. Kotliar, *First-principles calculations of the electronic structure and spectra of strongly correlated systems: dynamical mean-field theory*, J. Phys.: Condens. Matt. **9**, 7359 (1997).
11. A. I. Lichtenstein and M. I. Katsnelson, *Ab initio calculations of quasiparticle band structure in correlated systems: LDA++ approach*, Phys. Rev. B **57**, 6884 (1998).
12. E. Wimmer, H. Krakauer, M. Weinert, and A. J. Freeman, *Full-potential self-consistent linearized-augmented-plane-wave method for calculating the electronic structure of molecules and surfaces: O₂ molecule*, Phys. Rev. B **24**, 864 (1981).
13. M. Weinert, E. Wimmer, and A. J. Freeman, *Total-energy all-electron density functional method for bulk solids and surfaces*, Phys. Rev. B **26**, 4571 (1982).
14. D. Singh, *Planewaves, Pseudopotentials and the LAPW Method*, (Kluwer Academic Publishers, Boston/Dordrecht/London, 1994).
15. J. C. Slater, *Wave Functions in a Periodic Potential*, Phys. Rev. **51**, 846 (1937).
16. J. C. Slater, *Energy band calculations by the augmented plane wave method*, Advances in Quantum Chemistry **1**, 35 (1964).
17. T. Loucks, *Augmented Plane Wave Method*, (Benjamin, New York, 1967).
18. H. Bross, G. Bohn, G. Meister, W. Schubo, and H. Stohr, *New version of the modified augmented-plane-wave method*, Phys. Rev. B **2**, 3098 (1970).
19. O. K. Andersen, *Linear methods in band theory*, Phys. Rev. B **12**, 3060 (1975).
20. D. D. Koelling and G. O. Arbman, *Use of energy derivative of the radial solution in an augmented plane wave method: application to copper*, J. Phys. F (Metal Phys.) **5**, 2041 (1975).
21. R. V. Kasowski, *Band Structure of NiS as Calculated Using a Simplified Linear-Combination-of-Muffin-Tin-Orbitals Method*, Phys. Rev. B **8**, 1378 (1973).
22. P. M. Marcus, *Variational Methods in the Computation of Energy Bands*, Int. J. Quantum Chem. Suppl. **1**, 567 (1967).
23. M. Weinert, *Solution of Poisson's equation: beyond Ewald-type methods*, J. Math. Phys. **22**, 2433 (1981).
24. D. R. Hamann, *Semiconductor Charge Densities with Hard-Core and Soft-Core Pseudopotentials*, Phys. Rev. Lett. **42**, 662 (1979).
25. H. J. F. Jansen and A. J. Freeman, *Total-energy full-potential linearized augmented-plane-wave method for bulk solids: Electronic and structural properties of tungsten*, Phys. Rev. B **30**, 561 (1984).

26. S.-H. Wei, H. Krakauer, and M. Weinert, *Linearized augmented-plane-wave calculation of the electronic structure and total energy of tungsten*, Phys. Rev. B **32**, 7792 (1985).
27. S.-H. Wei and H. Krakauer, *Local-density-functional calculation of the pressure-induced-metalization of BaSe and BaTe*, Phys. Rev. Lett. **55**, 1200 (1985).
28. L. F. Mattheiss and D. R. Hamann, *Linear augmented-plane-wave calculation of the structural properties of bulk Cr, Mo, and W*, Phys. Rev. B **33**, 823 (1986).
29. P. Blaha, K. Schwarz, P. Sorantin and S.B. Trickey, *Full-potential, linearized augmented plane wave programs for crystalline systems*, Comp. Phys. Commun. **59**, 399 (1990).
30. see <http://www.flapw.de>
31. H. Krakauer, M. Posternak and A. J. Freeman, *Linearized augmented plane-wave method for the electronic band structure of thin films*, Phys. Rev. B **19**, 1706 (1979).
32. D. R. Hamann, L. F. Mattheiss and H. S. Greenside, *Comparative LCAO-LAPW study of Cl chemisorption on the Ag(001) surface*, Phys. Rev. B **24**, 6151 (1981).
33. E. Wimmer, H. Krakauer and A. J. Freeman, *Theory of surface electronic structure*, Adv. Electronics Electron Phys. **65**, 337 (1985).
34. In the scalar relativistic approximation (SRA)^{35,81-83} of the full relativistic Kohn–Sham equations the mass-velocity and Darwin terms are included to all orders of $(1/c^2)^n$, where c is the velocity of light, but the spin–orbit interaction is systematically omitted. In this approach the angular momentum quantum number ℓ and the spin quantum number σ remain good quantum numbers.
35. D. D. Koelling and B. N. Harmon, *A technique for relativistic spin-polarised calculations*, J. Phys. C (Solid State Physics) **10**, 3107 (1977).
36. C. Li, A. J. Freeman, H. J. F. Jansen, and C. L. Fu, *Magnetic anisotropy in low-dimensional ferromagnetic systems: Fe monolayers on Ag(001), Au(001), and Pd(001) substrates*, Phys. Rev. B **42**, 5433 (1990).
37. J. M. Soler and A. R. Williams, *Augmented-plane-wave forces*, Phys. Rev. B **42**, 9728 (1990).
38. R. Yu, D. Singh, and H. Krakauer, *All-electron and pseudopotential force calculations using the linearized-augmented-plane-wave method*, Phys. Rev. B **43**, 6411 (1991).
39. S. Blügel, *First Principles Calculations of the Electronic Structures of Magnetic Overlayers on Transition Metal Surfaces*, (Forschungszentrum Jülich, Jül. Report 2197, 1988).
40. D. Singh, *Simultaneous solution of diagonalization and self-consistency problems for transition–metal systems*, Phys. Rev. B **40**, 5428 (1989).
41. G. W. Fernando, *Iterative approaches to electronic structure with augmented bases*, Phys. Rev. B **41**, 903 (1990).
42. R. Wu and A. J. Freeman, *An efficient step–forward way to solve the Schrödinger eigenvalue equation in self-consistent calculations*, Comp. Phys. Comm. **76**, 58 (1993).
43. D. Singh, *Ground-state properties of lanthanum: Treatment of extended-core states*, Phys. Rev. B **43**, 6388 (1991).
44. E. Sjöstedt, L. Nordström, D. Singh, *An alternative way of linearizing the augmented plane-wave method*, Solid State Commun. **114**, 15 (2004).
45. Ph. Kurz, F. Förster, L. Nordström, G. Bihlmayer, and S. Blügel, *Ab initio treat-*

- ment of noncollinear magnets with the full-potential linearized augmented plane wave method*, Phys. Rev. B **69**, 024415 (2004).
46. Y. Mokrousov, G. Bihlmayer, and S. Blügel, *Full-potential linearized augmented plane-wave method for one-dimensional systems: Gold nanowire and iron monowires in a gold tube*, Phys. Rev. B **72**, 045402 (2005).
 47. M. Usuda, N. Hamada, T. Kotani, and M. van Schilfgaarde, *All-electron GW calculation based on the LAPW method: Application to wurtzite ZnO*, Phys. Rev. B **66**, 125101 (2002)
 48. D. Wortmann, H. Ishida, and S. Blügel, *An ab initio Green-function formulation of the transfer matrix: Application to complex bandstructures*, Phys. Rev. B **65**, 165103 (2002).
 49. D. Wortmann, H. Ishida, and S. Blügel, *An embedded Green-function approach to the ballistic electron transport through an interface*, Phys. Rev. B **65**, 165103 (2002).
 50. E. E. Krasovskii, *Augmented-plane-wave approach to scattering of Bloch electrons by an interface*, Phys. Rev. B **70**, 245322 (2004).
 51. M. L. Cohen, *Electronic structure of solids*, Phys. Rep. **110**, 293 (1984).
 52. W. E. Pickett, *Pseudopotential methods in condensed matter applications*, Comp. Phys. Rep. **9**, (1)15 (1989).
 53. H. Akai, M. Akai, S. Blügel, B. Drittler, H. Ebert, K. Terakura, R. Zeller, and P. H. Dederichs, *Theory of Hyperfine Interactions in Metals*, Prog. Theo. Phys. (Suppl) **101**, 11 (1990).
 54. M. Wuttig, Y. Gauthier, S. Blügel, *Magnetically Driven Buckling and Stability of Ordered Surface Alloys: Cu(100) c(2 × 2) Mn*, Phys. Rev. Lett. **70**, 3619 (1993).
 55. W. Kohn and L.J. Sham, *Self-Consistent Equations Including Exchange and Correlation Effects*, Phys. Rev. **140**, A1133 (1965).
 56. S. Blügel, *First Principles Calculations of the Electronic Structures of Magnetic Overlayers on Transition Metal Surfaces*, (PhD thesis, RWTH Aachen, 1988).
 57. L. Hedin and B. I. Lundqvist, *Explicit local exchange-correlation potentials*, J. Phys. C (Solid State Physics) **4**, 2064 (1971).
 58. S. H. Vosko and L. Wilk and N. Nusair, *Accurate spin-dependent electron liquid correlation energies for local spin density calculations: a critical analysis*, Can. J. Phys. **58**, 1200 (1980).
 59. J. P. Perdew, J. A. Chevary, S. H. Vosko, K. A. Jackson, M. R. Pederson, D. J. Singh, and C. Fiolhais, *Atoms, molecules, solids, and surfaces: Applications of the generalized gradient approximation for exchange and correlation*, Phys. Rev. B **46**, 6671 (1992)
 60. J. P. Perdew, K. Burke, and M. Ernzerhof, *Generalized Gradient Approximation Made Simple*, Phys. Rev. Lett. **77**, 3865 (1996).
 61. J. Stoer, *Numerische Mathematik I*, (Springer-Verlag, Berlin, 1994).
 62. D. J. Chadi and Marvin L. Cohen, *Special Points in the Brillouin Zone*, Phys. Rev. B **8**, 5747 (1973).
 63. S. L. Cunningham, *Special points in the two-dimensional Brillouin zone*, Phys. Rev. B **10**, 4988 (1974).
 64. O. Jepsen and O. K. Andersen, *The electronic structure of h.c.p. Ytterbium*, Solid State Commun. **9**, 1763 (1971).
 65. G. Lehmann and M. Taut, *On the Numerical Calculation of the Density of States and*

- Related Properties*, phys. stat. sol. (b) **54**, 469 (1972).
66. P. E. Blöchl, O. Jepsen, and O. K. Andersen, *Improved tetrahedron method for Brillouin-zone integrations*, Phys. Rev. B **49**, 16223 (1994).
 67. R. Pentcheva, *Ab-initio Rechnungen zum Zusammenhang zwischen Magnetismus und Struktur ultradünner Filme*, (Diploma thesis, RWTH Aachen, 1995).
 68. A. R. Williams, J. Kübler, and C. D. Gelatt Jr., *Cohesive properties of metallic compounds: Augmented-Spherical-Wave calculations*, Phys. Rev. B **19**, 6094 (1979).
 69. T. Takeda and J. Kübler, *Linear augmented plane wave method for self-consistent calculations*, J. Phys. F **9**, 661 (1979).
 70. S. Goedecker, *Treatment of semicore states in the linearized augmented-plane-wave method and other linearized electronic-structure methods*, Phys. Rev. B **47**, 9881 (1993).
 71. J. Yu, A. J. Freeman, R. Podloucky, P. Herzig, and P. Weinberger, *Origin of electric-field gradients in high-temperature superconductors: $YBa_2Cu_3O_7$* , Phys. Rev. B **43**, 532 (1991).
 72. E. E. Krasovskii and W. Schattke, *The extended-LAPW-based $\mathbf{k}\cdot\mathbf{p}$ method for complex band structure calculations*, Solid State Comm. **93**, 775 (1995).
 73. E. E. Krasovskii, *Accuracy and convergence properties of the extended linear augmented-plane-wave method*, Phys. Rev. B **56**, 12866 (1997).
 74. G. K. H. Madsen, P. Blaha, K. Schwarz, E. Söstedt, and L. Nordström, *Efficient linearization of the augmented plane-wave method*, Phys. Rev. B **64**, 195134 (2001).
 75. J. D. Jackson, *Klassische Elektrodynamik* (Walter de Gruyter, Berlin, New York, 1983).
 76. W. Ning, C. Kailai, and W. Dingsheng, *Work Function of Transition-Metal Surface with Submonolayer Alkali-Metal Coverage*, Phys. Rev. Lett. **56**, 2759 (1986).
 77. J. Tersoff and D. R. Hamann, *Theory and Application for the Scanning Tunneling Microscope*, Phys. Rev. Lett. **50**, 1998 (1983).
 78. S. Heinze, S. Blügel, R. Pascal, M. Bode, R. Wiesendanger, *Prediction of Corrugation Reversal in STM-images of bcc-(110)-surfaces: $W(110)$, $Ta(110)$, $Fe(110)$* , Phys. Rev. B **58**, 16432 (1998).
 79. P. Blaha, K. Schwarz, P. Dufek, and R. Augustyn, WIEN95 (Technical University, Vienna, 1995).
 80. M. Petersen, F. Wagner, L. Hufnagel, and M. Scheffler, *Improving the efficiency of FP-LAPW calculations* Comp. Phys. Comm. **126**, 294 (2000).
 81. T. Takeda, *The scalar relativistic approximation*, Z. Physik B **43**, 32 (1978).
 82. J. H. Wood and A. M. Boring, *Improved Pauli Hamiltonian for local-potential problems*, Phys. Rev. B **18**, 2701 (1978).
 83. H. Gollisch and L. Fritsche, *Relativistic one-particle equation for electron states of heavy metals*, phys. stat. sol. (b) **86**, 145 (1978).